We thank the reviewers for their constructive comments and suggestions. We have given full consideration to the comments in the revised manuscript. Please find below a point-by-point reply to the questions raised. Please note that in addition to the reviewer comments we have added a sentence in the acknowledgements: “The authors thank the two anonymous reviewers for their constructive comments and suggestions.”

Reviewer #1:

Review: HadGEM3-GC3.1 atmospheric-only simulations are assessed to discuss the impacts of horizontal resolution increasing on the precipitation climatology and precipitation variabilities (in intensity and in the space and time) over South America. Three ensembles of HadGEM3-GC3.1 with horizontal grid spacing of approximately~130(N96), 60 (N216) and 25 km (N512) are compared with reanalysis (NCEP and ERA-Interim) and satellite data (CMORPH) to evaluate the impacts of resolution on precipitation using different metrics (climatology, seasonality, large scale influences of MJO and ENSO, coupling between precipitation and soil moisture, intensity distribution, dry spells, etc.). The results are new and very relevant since are showing that improvements on precipitation occur when the resolution is increased from N96 to N216 for most regions of South America, while over the Andes Mountains the improvements continue until N512. The improvements are associated with better simulation of moisture flux convergence and daily precipitation distribution at fine resolution. In addition, the authors do not found any relevant impacts of resolution on low-frequency variability of precipitation (MJO and ENSO forcings). Overall, this study contributes to under-standing the impacts of model resolution on precipitation at spatial and temporal and some limitation of resolution refinements. The manuscript has new contributions to the atmospheric modeling area and it is worthy of publishing after some minor revisions.

Minor comments

In some parts of the text appear “north-east”, “south-east” and in others, respectively, “northeast”, “southeast” to refer to the same geographical regions in Brazil ((Lines: 16,17, 31, 32, 43,..., 504, 508, L514,...). Please, to unify how to refer to these regions preferentially using “northeast” and “southeast”

Thank you for your comment, we have rephrased the text, using northeast and southeast instead of north-east and south-east.

L32, L51, L82 – “de Souza Custodio et al. 2017)” to “Custodio et al. 2017)”

We have changed the reference throughout text, editing the reference to Custodio et al. (2017).

L38 – to remove “over South America”

We have removed “over South America”

L57 – In relation to the “South American Monsoon System â˘Ä´Í...” to refer to Vera et al.(2006). Vera, C., et al. (2006), A unified view of the American monsoon systems, J.Clim., 19, 4977–5000.

Thank you for the reference, we have now added Vera et al. (2006) in the main text.

L103 – should be “improves the modeled precipitation variability over...”

We have changed the sentence accordingly to your comment.

L142-143 – Please, to include the information of what are the horizontal resolutions of GPCC, University Delaware, NCEP-NCAR and ERA-Interim.

Both GPCC and UDEL precipitation are provided on a 0.5° horizontal resolution. NCEP-NCAR is gen at a 2.5° horizontal resolution and ERA-interim at a 1.5° horizontal resolution. This information has been added to the data section (Sect. 2.2). Please see: “To evaluate time-mean rainfall and sub-seasonal to seasonal variability, we compare HadGEM3 to longer-period, but lower-resolution, gauge-based datasets from the University of Delaware (Willmott et al. 2001) and from the Global Precipitation Climatology Centre (GPCC; Schneider et al. 2014), both at a 0.5° horizontal resolution. We assess mean circulation against the NCEP-NCAR reanalysis (Kanamitsu et al. 2002), given on a 2.5° resolution (144 × 72) with 17 vertical levels, and ERA-interim reanalysis (Dee et al. 2011), given on a 1.5° horizontal resolution.”

L146 – The citation of ERA-Interim in this context is wrong since it is available only from 1979. Please, check.

Thank you for your comment. This is a mistake, we have used NCEP to assess biases in monthly mean wind. The sentence has been corrected.

L194 – I suggest to change “over the equator...” to “over tropical latitudes...”\

We have changed “over the equator” to “over tropical latitudes”.

L195 – “eastern Brazil is relatively dry” should be “northeastern Brazil is relatively dry” since in subtropical eastern of Brazil precipitation is between 4-6 mm/day, which cannot be considered dry

Thank you for you comment, we have rephrased the text following your suggestion.

L231- Is hard to interpret Figures 2d-e-f since they do not show any important difference over the continent. This occurs because they are using the same scale of Figures2-a-b-c. I suggest to the authors to remove Figures 2d-e-f or to change the scale to illustrates what is important in terms of evapotranspiration over continental areas.

Our point is here to show that effect of the resolution it not mediated by changes in evaporation, and that effect on precipitation is primary due to large-scale changes rather than to local changes. Therefore, we think that it is important to keep the changes in evaporation in the main text. We do prefer to keep the same scale to compare changes in moisture flux convergence and evaporation so that both fields are easily comparable. We agree that patterns in evaporation but this is due to the fact that changes in evaporation are rarely significant and that changes in precipitation are most only due to changes in moisture flux convergence.

L346– change “1, 7 and 8...” to “1, 7 and 8 (Fig. 6a-g-h)...”

We have corrected the typo.

L386 – change to “moisture flux convergence...”

We have rephrased the sentence, using “moisture flux convergence” instead of “moisture convergence”.

L395 – “over eastern Brazil...” should be “over eastern Brazil and southeastern South America “

Thank you for your comment, we have added “and southeastern South America” in the sentence.

L416 – I am seeing overestimation in Figure 9e over northeastern Brazil (the box to east 45oW and north 15oS) and not over “eastern Brazil”. Please, verify the affirmation.

We have rephrased the sentence, changing “eastern Brazil” by “northeastern Brazil”.

L457-459 – Please, check the letters of Figures 10 and 12: a) L457 “Fig. 10c and Fig.10e” should be “Fig. 10h and Fig. 10j”; b) L458 “Fig. 10e; Fig. 12g” should be “Fig.10g; Fig 12e”; c) L459 “Fig. 10e; Fig. 12h-j” should be “Fig. 10h-j; Fig. 12e”.

We have rephases the text, correcting “Fig. 10c and Fig. 10e” by “Fig. 12c and Fig. 12e”, “Fig. 10e; Fig. 12g” by “Fig.10g; Fig 12e”, and “Fig. 10e; Fig. 12h-j” by “Fig. 10h-j; Fig. 12e”.

L461 – The correct location are “Peruvian Andes, Paraguay, and northeastern Argentina”
We have rephrased the sentence, changing “eastern Argentina” by “northeastern Argentina”.

L475 – “function of time (Fig. 13a-d) and distance (Fig. 13e-h)...” should be “function of distance (Fig. 13a-d) and time (Fig. 13e-h)”

Thank you to pointing this mistake out. We have corrected the text.

L489 – “precipitation features...” should be “simulated precipitation features...”

We have rephrased the text following your suggestion.

Reviewer #2:

The manuscript is very well written, the figures have high quality, and I believe the authors already answered most of the concerns from the reviewers. However, I would like to propose just one more discussion, which is related to Line 78 and seasonal precipitation predictability.

Jia et al. (2015) suggests that higher atmospheric and land resolution "can" improve seasonal forecasts when combined with statistical analysis. Bombardi et al. (2019) performed a somewhat similar analysis to this manuscript, but focusing on summer precipitation predictability using the IFS (ECMWF) model. They found no significant improvement in seasonal predictability of summer precipitation due to an increase in resolution. Although there seems to be some value in increasing the resolution of the both the atmosphere and the ocean. There is some consensus in the scientific community that an increase in spatial resolution without an appropriate improvement of model physics does not lead to better forecasts, because the increase in resolution leads to an increase in noise. I don't expect the authors to perform any more analysis, I would just like to ask the authors to perhaps include a discussion on how their findings related to studies that focus on precipitation predictability (e.g. Becker et al. 2014; Jia et al. 2015; Bombardi t al. 2019). The argument here is that an increase in spatial resolution leads to an improvement of the model's representation of precipitation. Right. But ultimately, we want the model to be able to predict precipitation. Considering the computational cost of climate simulations and potentially negative effects of increasing spatial resolution, should we really advocate for simulations to be performed with higher spatial resolution? Just some thoughts on the matter would suffice.

Becker, E., H.van den Dool, and Q.Zhang, 2014: Predictability and forecast skill in NMME. J. Climate, 27, 5891–5906, https://doi.org/10.1175/JCLI-D-13-00597.1.

Bombardi, R. J., L. Trenary, K. Pegion, B. Cash, T. DelSole, and J. L. Kinter, 2018: Seasonal Predictability of Summer Rainfall over South America. J. Climate, 31, 8181– 8195,

We thank the reviewers for their constructive comments and suggestions. We have given full consideration to the comments in the revised manuscript. We have added a short discussion in the paper, following your suggestion, and have included the citation to Bombardi et al. (2018).

Please see, lines 565-568: “Although we hypothesized that increasing resolution might affect the ability of climate models to predict precipitation, Bombardi et al. (2018) have shown that an improvement of South American precipitation prediction due to an increase in resolution is not straightforward. In addition to resolution, further works should, therefore, be devoted to understanding the effects of physic, on prediction system performance.”

Role of atmospheric horizontal resolution in simulating tropical and subtropical South American precipitation in HadGEM3-GC31

Paul-Arthur Monerie[1], Amulya Chevuturi[1], Peter Cook[1], Nick Klingaman[1], Christopher E. Holloway[2]

[1] Department of Meteorology, National Centre for Atmospheric Science (NCAS), University of Reading, Reading, UK

[2]Department of Meteorology, University of Reading, Reading, UK

Correspondence to: Paul-Arthur Monerie (pmonerie@gmail.com)

Abstract

We assess the effect of increasing horizontal resolution on simulated precipitation over South America in a climate model. We use atmosphere-only simulations, performed with HadGEM3-GC31 at three horizontal resolutions: N96 (~130 km, 1.88° x 1.25°), N216 (~60 km, 0.83° × 0.56°), and N512 (~25 km, 0.35° x 0.23°). We show that all simulations have systematic biases in annual mean and seasonal mean precipitation over South America (e.g. too wet over the Amazon and too dry in northeast). Increasing horizontal resolution improves simulated precipitation over the Andes and northeast Brazil. Over the Andes, improvements from horizontal resolution continue to ~25km, while over northeast Brazil, there are no improvements beyond ~60km resolution. These changes are primarily related to changes in atmospheric dynamics and moisture flux convergence. Over the Amazon basin, precipitation variability increases at higher resolution. We show that some spatial and temporal features of daily South American precipitation are improved at high resolution, including the intensity spectra of rainfall. Spatial scales of daily

precipitation features are also better simulated, suggesting that higher resolution may improve the representation of South American mesoscale convective systems.

1. Introduction

South America is a large area encompassing tropical, sub-tropical and extratropical climates. The Andes covers western South America, from South to North, while the eastern part of South America is flatter than the west. The Amazon basin has high mean rainfall and is covered by a rainforest, while northeastern Brazil is semi-arid. Several climatic areas are thus often defined to account for the climatic heterogeneity of South America, with focus specifically on the Andes, the Amazon Basin, northeast Brazil and southeast Brazil (Custodio et al. 2017).

Climate models have biases in simulating South American precipitation, partly due to biases in simulating teleconnections between both Atlantic and Pacific sea-surface temperatures (SSTs), and precipitation over land (Bombardi and Carvalho 2008; Jung et al. 2011; Yin et al. 2013; Sierra et al. 2015; Coelho et al. 2016; Koutroulis et al. 2016). At sub-seasonal scales, precipitation variability is associated with the Madden—Julian Oscillation (MJO) (Grimm 2019). The MJO modulates precipitation over South America, leading to either anomalously dry or wet conditions, depending on its phase. The MJO also favors extreme events, leading to droughts and floods (Grimm 2019). At inter-annual scales, the El Niño Southern Oscillation (ENSO) strongly impacts Amazon precipitation, with El Niño events related to droughts (Grimm and Silva Dias 1995; Zeng et al. 2008; Marengo et al. 2008, 2011, 2013; Grimm and Tedeschi 2009; Lewis et al. 2011). Variability in the tropical Atlantic Ocean modulates trade easterlies and impacts precipitation over northeast Brazil (Liu and Juárez 2001; Zeng et al. 2008) and southeast Brazil (Coelho et al. 2016). On decadal to multi-decadal scales, variability in northeast Brazilian precipitation is tied to the Atlantic Multidecadal Variability, which is associated with the location of the Atlantic Intertropical Convergence Zone (ITCZ) (Knight et al. 2006). Brazilian precipitation is also associated with Interdecadal Pacific

47 Variability (IPV; Power et al. 1999), positive IPV phases reduce precipitation over South America
48 (Villamayor et al. 2018). Errors in simulating teleconnections from local and remote SST variability leads
49 to biases in the intensity, position of the ITCZ and the South Atlantic Convergence Zone (SACZ), which
50 degrade simulated South American precipitation and temperature (Bombardi and Carvalho 2008; Custódio
51 et al. 2012; Custodio et al. 2017).

52 Besides teleconnections, climate variability results from complex local interactions between energy,
53 precipitation and soil moisture. These feedbacks are particularly strong over interior South America, one
54 of the "hot spots" in soil moisture—precipitation coupling (Koster et al. 2004; Wei and Dirmeyer 2012).
55 Variability in recycling accounts for a large fraction of precipitation variability over northeastern Brazil
56 and the La Plata Basin (Sörensson and Menéndez 2011). Soil moisture memory influences atmospheric
57 variability and could affect the development of the South American Monsoon System (Vera et al. 2006).
58 Therefore, biases in simulated South American climate may be partly attributed to biases in local land-
59 atmosphere coupling.

60 Improving simulated precipitation in climate models may also improve subseasonal-to-decadal predictions,
61 because the performance of initialised forecasts and free-running models relies on the representation of key
62 physical processes, such as convection and land-atmosphere feedbacks. For instance, models with the
63 largest systematic errors produce the lowest precipitation prediction performance (DelSole and Shukla
64 2010). Jia et al. (2014) showed that the high-resolution version of the GFDL model produces lower biases
65 and higher skill for seasonal variations of 2-m air temperature and precipitation over South America, than
66 its lower-resolution counterpart. Therefore, Doblas-Reyes et al. (2013) proposed that increasing spatial
67 resolution is one of the main challenges for improving predictions.

68 Horizontal resolutions of Coupled Model Intercomparison Project (CMIP; Taylor et al. 2012; Eyring et al.
69 2016) models are typically ~150 km, or coarser, in the atmosphere, and ~100 km in the ocean. Important
70 climate processes, such as atmospheric convection, and mesoscale boundary currents and eddies, have to

71 be parameterized rather than resolved, which may compromise dynamical processes and dynamics-physics
72 interactions (Collins et al. 2018). A growing body of evidence shows then that increasing horizontal
73 resolution can improve some aspects of the simulated climate (Roberts et al. 2018, 2019; among others).
74 Higher-resolution ocean-atmosphere coupled models outperform lower-resolution models at simulating
75 SST over coastal upwelling regions, due to a better simulation of near-surface wind and its effect on the
76 ocean (Shaffrey et al. 2009; Gent et al. 2010; McClean et al. 2011; Delworth et al. 2011; Sakamoto et al.
77 2012; Small et al. 2014). Resolution reduces the double ITCZ bias (Delworth et al. 2011) and improves
78 variability in the El-Niño Southern Oscillation (Shaffrey et al. 2009; Sakamoto et al. 2012; Small et al.
79 2014) and north Atlantic SSTs (Gent et al. 2010). Jung et al. (2011) and Jia et al. (2014) highlighted that
80 increased resolution improved simulated South American precipitation and tropical mean precipitation, and
81 atmospheric circulation. Improved land precipitation is partly due to a better representation of orography
82 (Gent et al. 2010; Delworth et al. 2011; Sakamoto et al. 2012). Over South America, increasing horizontal
83 resolution improves the representation of climate patterns (Custodio et al. 2017), particularly over the
84 Ocean, over the Atlantic ITCZ and SACZ. Although strongly model and season dependent, high resolution
85 regional climate models also improve simulated precipitation and temperature over South America (Falco
86 et al. 2019; Solman and Blázquez 2019). Increased resolution also affects local features, such as the
87 propagation of mesoscale systems (Vellinga et al. 2016) and local land-atmosphere feedbacks (Mueller et
88 al. under review).

89 However, horizontal resolution does not always improve simulated climate. Bacmeister et al. (2013) found
90 that the high-resolution Community Atmosphere Model (CAM) did not improve simulated South American
91 rainfall, compared to a lower-resolution configuration. Some simulations exhibit too much warming and
92 cooling, especially over polar regions where sea ice is not accurately represented (McClean et al. 2011;
93 Kirtman et al. 2012). Impacts of increased horizontal resolution strongly depend on the range of resolutions
94 considered, on the region, phenomena and spatial and temporal scales of interest (Jung et al. 2011; Roberts

95 et al. 2018). Therefore, there is a need to better understand how increasing the horizontal resolution could
96 benefit simulated South American precipitation.

97

98

99 Accurate predictions and projections of extreme rainfall require realistic simulated precipitation
100 distributions. However, models exhibit biases in the frequency and persistence of light (<10 $mm.day^{-1}$) and
101 heavy precipitation (>20 $mm.day^{-1}$) (Sun et al. 2006; Dai 2006; Koutroulis et al. 2016). Errors in
102 precipitation frequency and intensity are related to biases in the global hydrological cycle, including
103 evaporation recycling over land (Trenberth 2011; Demory et al. 2014). Improved representations of intense
104 small-scale events improves modelled precipitation variability in models over parts of South America (De
105 Sales and Xue 2011). These biases may be partly due to the coarse resolution of CMIP climate models;
106 increased resolution could improve simulated extreme convective rainfall by enhancing smaller-scale
107 precipitation features, as shown by Solman and Blázquez (2019) over South America.

108 High resolution models are costly; if higher resolution produces little or no improvements in model biases,
109 then computational resources could be used elsewhere, such as in increased ensemble size or adding
110 initialization dates in forecasting systems, or improved or additional model physics. The European Union's
111 Horizon 2020 PRIMAVERA project (www.primavera-h2020.eu) uses the CMIP6 High Resolution Model
112 Intercomparison Project (HighResMIP; Haarsma et al. 2016) protocol and aims to develop a new generation
113 of advanced high-resolution global climate models.

114 We use PRIMAVERA simulations to evaluate whether increased horizontal resolution improves simulated
115 South American precipitation. We address three main questions:

116 - What are the model biases in simulated precipitation over South America?

- Is South American mean precipitation and variability better simulated at higher than at lower resolution? What is the minimum resolution required to improve the lower resolution biases?

- Are the spatial and temporal organizations of precipitation, better simulated at higher resolution?

The paper is structured as follows: the model, data and methodology are described in Sect. 2. Sect. 3 focuses on the model's ability to simulate annual and seasonal precipitation mean. We discuss seasonal to interannual variability in Sect. 4 and daily to sub-seasonal variability and spatial and temporal scales of precipitation in Sect. 5. A conclusion is given in Sect. 6.

2. Data and Methods

2.1 HadGEM3-GC3.1

HadGEM3-GC3.1 (hereafter HadGEM3) (Williams et al. 2018) has been run in an atmosphere-only configuration for 1950-2014, forced by HadISST2 daily 0.25° SSTs and sea ice (Rayner et al. 2006). The atmospheric model is the Global Atmosphere 7.1 scientific configuration (Walters et al. 2019), with 85 vertical levels. A common historical forcing is imposed in all simulations, including SSTs, greenhouse gases and aerosols. Three sets of simulations are performed, which only differ by their horizontal resolution and by a stochastic perturbation of their initial conditions: N96 horizontal resolution (~130 km, 1.88° x 1.25°; HadGEM3-GC3.1-LM), N216 horizontal resolution (~60 km, 0.83° × 0.56°; HadGEM3-GC3.1-MM) and N512 horizontal resolution (~25 km, 0.35° x 0.23°; HadGEM3-GC3.1-HM). Three members were performed at each resolution, for a total of 9 simulations. The simulations are part of the European Union's Horizon 2020 PRIMAVERA project (www.primavera-h2020.eu) uses the CMIP6 High Resolution Model Intercomparison Project (HighResMIP; Haarsma et al. 2016).

2.2 Observations and reanalysis

To verify the spatial and temporal scales of rainfall, three-hour and daily mean precipitation from HadGEM3 is compared against a high-resolution (0.25° x 0.25°) satellite-derived product for 1998-2017: NOAA CPC Morphing Technique (CMORPH version 1; Joyce et al. 2004). To evaluate time-mean rainfall and sub-seasonal to seasonal variability, we compare HadGEM3 to longer-period, but lower-resolution, gauge-based datasets from the University of Delaware (Willmott et al. 2001) and from the Global Precipitation Climatology Centre (GPCC; Schneider et al. 2014), both at a 0.5° horizontal resolution. We assess mean circulation against the NCEP-NCAR reanalysis (Kanamitsu et al. 2002), given on a 2.5°

148 resolution (144 × 72) with 17 vertical levels, and ERA-interim reanalysis (Dee et al. 2011), given on a 1.5°
149 horizontal resolution.

150 To assess biases and impacts of the horizontal resolution on mean annual and seasonal precipitation we
151 used monthly data, over 1950-2014, using GPCC and NCEP reanalysis. For daily variance we used GPCC,
152 over 1982-2014. For the analysis of the spatial scales in precipitation, we used CMORPH, over 1998-2014.
153 Note that results in mean and variance in precipitation were also assessed with CMORPH, in addition to
154 GPCC, for a consistency with the spatial scales analysis.

155 2.3 Data interpolation

156 Differences between HadGEM3 and observations and between HadGEM3 at different horizontal
157 resolutions are assessed by first interpolating all data to a common 0.5° x 0.5° resolution. Results were
158 repeated, with data interpolated onto a common coarser resolution, 2.5° x 2.5° grid, showing similar results.
159 For the analysis of the spatial scales in precipitation, both simulations and observations are interpolated
160 onto a common lower resolution, N96.

161 2.4 Analysis of Scales of Precipitation (ASoP)

162 The Analysis of Scales of Precipitation (ASoP; Klingaman et al. 2017; Martin et al. 2017) diagnostics
163 provide information on the intensity spectra of precipitation, the contribution to total precipitation from
164 precipitation events of various intensities, the temporal persistence of precipitation and the typical spatial
165 and temporal scales of precipitation.

166 The intensity spectra measures intensity distributions by computing the contributions of discrete intensity
167 bins to the total precipitation for each grid point, to be visualised as maps (at grid scale) or aggregated over
168 regions into histograms. Spatial scales of precipitation features are measured by dividing the analysis
169 domain into non-overlapping subregions and computing correlations of each point in the sub-region against

the central grid point, then averaging the resulting correlation maps over all sub-regions. Temporal scales are measured by auto-correlations at a range of lags. Further information can be found in Klingaman et al. (2017) and Martin et al. (2017).

Further, we measure the distribution of the duration of precipitation events in discrete intensity bins by constructing a two-dimensional (2-D) histogram of binned precipitation intensity against binned duration in that intensity bin. We calculate the 2-D histogram by aggregating data across the analysis domain, then normalised by the number of spatial and temporal points in the dataset, to compare across datasets. The ASoP and duration diagnostics are applied over two subregions of South America: Amazon (AMZ; 10°S – 5°N; 72°W – 50°W) and southeast South America (SESA; 35°S – 18°S; 63°W – 40°W). We apply these diagnostics to daily data on the native HadGEM3 and CMORPH grids, as well as a common N96 grid.

We produce a 1-D histogram for duration of dry spells, where a dry spell is defined as a time interval of consecutive precipitation events of less than 0.1 $mm.day^{-1}$. This histogram is normalized by number of spatial and temporal points in the dataset, to compare across datasets.

2.5 Coupling strength metric

Interactions between soil moisture, precipitation, temperature and evaporation modulate climate variability. We assess the sensitivity of coupling strength between these variables to resolution. Coupling strength is defined, at each grid point, after removing the linear trend and seasonal cycle, and on the daily time scale, as

$$r_{a,b}\sigma_b = cor(a,b) \times std(b)$$

Where *cor(a, b)* is the correlation between the variables *a* and *b* and *std* is the standard deviation. As an example, for the coupling strength between soil moisture (in the top 0.1m of soil) and latent heat flux, *a* is the soil moisture, and *b* is the latent heat flux. The linear trend was removed over all days, selecting DJF

193 months only, and across all years to define anomalies relative to the seasonal cycle. We only selected days
194 over the DJF season, between 1950 and 2014. The coupling strength is also computed with a 2-day lag
195 correlation.
196
197
198 # 3 Interannual and seasonal means
199 ## 3.1 interannual mean

200 Observed annual mean precipitation is high over the tropical latitudes, i.e. the Amazon Basin, Colombia
201 and South Venezuela, while northeastern Brazil is relatively dry (Fig. 1a). Precipitation is stronger over the
202 eastern side of the Andes than over the western side, because moisture is carried across South America by
203 the trade easterlies. Over the Andes, peaks in precipitation are collocated with the orography.

204 HadGEM3 has clear deficiencies in simulating precipitation, particularly over high orography. N96 has a
205 wet bias over southern Brazil and over the Andes, from 30°S to the equator, and a dry bias over northeast
206 Brazil (Fig. 1b). Biases are strong, up to 3 $mm.day^{-1}$ over the Andes. The dry bias over the northeast Brazil
207 is associated with anomalously weak easterlies (Fig. 1b). An anomalously strong cyclonic circulation,
208 located over Peru, weakens the easterlies, between 10°S and the equator, decreasing moisture flux
209 divergence over the western Amazon Basin associated with a wet bias there (Fig. 1b). There is an
210 anomalously strong anticyclonic circulation, over southeast Brazil, which is associated with stronger
211 easterlies from the South Atlantic Ocean to southern Brazil and a wet bias (Fig. 1b).
212
213 N216 and N512 also show, wet biases over the Andes and southeastern Brazil, and dry biases over northeast
214 Brazil (Fig. 1c and Fig, 1d). Biases in low-level winds are also very similar in N96, N216 and N512. We
215 highlight the impacts of each step change in resolution by displaying differences between all pairs of
216 simulations. The total impact of shifting from N96 to N512 is given by N512-N96; intermediate steps are
217 illustrated by N216-N96 and N512-N216. This helps to define the minimum resolution required to extract

substantial simulation improvements, from the available sets of simulations. The strongest impact of increasing resolution is over the Andes, where N512-N96 reaches up to 2 $mm.day^{-1}$ (Fig. 2c). Significant differences are also obtained over the Amazon Basin, northeast Brazil and northwest Argentina (Fig. 2a-c). Over the Amazon basin and the Andes, changes in precipitation in N512-N96 are due to both N216-N96 and N512-N216 (Fig. 2a and Fig. 2b). In addition, differences consist of reduced precipitation (Fig. 2abc), and thus in reduced wet biases, over the Andes (Fig. 1bcd; see the stippling). Therefore, it is worth increasing horizontal resolution to N512 for simulating precipitation over the Andes.

Over northern Argentina, significant changes are only due to N216-N96 (Fig. 2a), while there are no significant changes in N512-N216 (Fig. 2b). Over the Amazon Basin, significant changes are found in both N216-N96 and N512-N216. Over the Amazon Basin and northern Argentina, increasing resolution increases precipitation, which strengthens the N96 wet bias. Over northeastern Brazil, the significant increase in precipitation with resolution reduces the N96 dry bias. However, the improvement is primarily found in N216-N96; resolutions higher than N216 do not appear to be useful. Over the Ocean, increased resolution is associated with strong changes in precipitation, i.e. precipitation increases over the eastern Pacific Ocean and decreases over the tropical Atlantic Ocean (especially just offshore of most coastal regions) (Fig. 2), but most of the effect comes from moving from N96 to N216.

Changes in evaporation with resolution are significant over the eastern Pacific Ocean, and over the southwest Atlantic Ocean, along the coast of South America (Fig. 2d-f). However, increasing resolution leads to only moderate changes in evaporation over land. Unlike evaporation, differences in moisture flux convergence (i.e. precipitation minus evaporation) are strong over both land and ocean (Fig. 2g-i). Therefore, the sensitivity of Amazon Basin and Andes precipitation to resolution is mostly due to sensitivity in moisture transport rather than in local moisture recycling (i.e. conversion of local evaporation into precipitation). This is consistent with Vannière et al. (2019), which showed that ocean-to-land moisture advection increases with resolution. We show small changes in specific humidity and surface air

temperature over land (Fig. S1 and Fig. S2). This suggests that changes in precipitation with resolution are due to dynamic changes, rather than thermodynamic changes. Increased resolution is associated with an eastward shift, toward the coast, of the southeast Pacific anticyclonic circulation (Fig. 2g-i) in the southern Pacific coastal region. The wind speed then strengthens and increases evaporation (Fig. 2d-f) and decreases moisture convergence (Fig. 2g-i). Over land, changes in wind speed are particularly strong over the mountains.

3.2 Seasonal means

We next examine the influence of resolution on seasonal rainfall, motivated by the strong seasonal cycle of South American rainfall (i.e., heavy rainfall over northern South America in July-September, while the Amazon basin is wetter in DJF than in JAS). Over northeast Brazil, the resolution sensitivity is strongest in DJF and MAM, mainly due N216-N96 (Fig. 3a; Fig. 3c; Fig. 3d and Fig. 3f), while the N512-N216 differences are moderate (Fig. 3b and Fig. 3e). Differences are also strong over the Amazon Basin, in DJF and SON, where increased resolution increases mean precipitation (Fig. 3c and Fig. 3l). Changes in Amazon Basin precipitation are contributed by both N216-N96 (Fig. 3a and Fig. 3j) and N512-N216 (Fig. 3b and Fig. 3k).

Over southwestern Brazil—northern Argentina, increasing resolution increases precipitation in all seasons which increases the wet bias. These changes are only due to N216-N96 (Fig. 3). Strong differences are also obtained over the tropical Pacific and Atlantic Ocean, from March to November (Fig. 3d, Fig. 3g and Fig. 3j), mainly due to N216-N96. N512-N216 does not strongly affect oceanic precipitation (Fig. 3e, Fig. 3h and Fig. 3k).

Improvements are shown over northeast Brazil in DJF and MAM. There is little sensitivity to resolution elsewhere in South America. Over the Amazon, changes are stronger in austral summer (i.e. DJF), during the monsoon, but biases are higher at high resolution.

4. Seasonal to interannual variability and teleconnections

We have shown a limited effect of resolution on mean precipitation. However, climate variability could be more sensitive to resolution because resolution may affect how the model simulates precipitation distribution, local and large-scale atmospheric dynamics, land-atmosphere coupling and mesoscale systems. Assessing climate variability provides useful information on the ability of climate models to simulate the climate system.

The pattern in annual precipitation variance follows the pattern in annual mean precipitation, i.e. higher along the equator than over the surrounding regions (Fig. 4a). At all resolutions, HadGEM3 overestimates precipitation variability over southeast Brazil, and underestimates precipitation variability between 15°S and the equator (Fig. 4b-d). HadGEM3 overestimates both mean precipitation and precipitation variability over parts of the Andes and southeast Brazil/northern Argentina (Fig. 1b-d and Fig. 4b-d). HadGEM3 has a mean wet bias but underestimates the precipitation variability over the Amazon Basin, although increasing resolution reduces the variability bias (Fig 4.e-g). Over southeast Brazil, increasing resolution slightly reduces the overestimation of precipitation variance (Fig. 4e-g). There are no changes in precipitation variance over northeast Brazil, in N512-N96 (Fig. 4e, Fig. 4f and Fig. 4g).

Precipitation variance also increases with resolution for individual seasons (not shown). Because both Pacific and Atlantic SSTs affect seasonal-to-interannual South American precipitation variability, we hypothesized that changes in variance to be associated with a change in the strength of the teleconnection between ENSO and South American precipitation, and between the South Atlantic SSTs and South American precipitation. However, this hypothesis was not supported by the following evidences: The

297 impact of ENSO on South America is assessed through regressing the El Niño 3.4 index (170-120°W; 5°S-
298 5°N) onto precipitation for each grid point, focusing on the seasonal anomalies (Fig. S3). We found that
299 increasing horizontal resolution does not systematically alter the influence of ENSO on Brazilian
300 precipitation. These analyses were repeated, focusing on tropical Atlantic gradients in SST, yielding a
301 similar conclusion to the one for ENSO, i.e. increasing the horizontal resolution does not change impacts
302 of the SST on precipitation over land (not shown).
303

5. Daily to sub-seasonal variability and teleconnections

5.1 Daily variability

Daily precipitation variance is more sensitive to resolution that monthly or annual variance. Over the Amazon Basin, differences between the simulations are stronger in austral summer than other seasons (Fig. S4). Besides, precipitation variability is strongly tied to the South American summer monsoon, which mainly occurs in DJF. Therefore, we focus further analysis on daily variance and on DJF.

In DJF, N96 underestimates daily precipitation variance (Fig. 5a). N216 and N512 outperform N96, with a reduced underestimation of precipitation variance over the Amazon Basin (Fig. 5b and Fig. 5c). The increase in variance is due to shifts from N96 to N216 and N216 to N512 (Fig. 5d and Fig. 5e). The difference in P-E variance is high, close to the difference in P variance (Fig. 5g; Fig. 5h and Fig. 5i). Therefore, changes in precipitation variance are mostly associated with changes in the variance of moisture flux convergence.

Biases in DJF daily precipitation variance have also been assessed using CMORPH over 1998-2014. The same conclusions are drawn: N96 underestimates variance and N512 overestimates variance (Fig. S4). However, the N96 biases are much reduced when compared to CMORPH instead of GPCC, such that N96 outperforms N216 and N512 (Fig. S4 and Fig. S5). In addition, the northern Brazil circulation is dominated by easterlies (Fig. 1a), whose variability reinforces by increasing the horizontal resolution (Fig. S6). Over southern Brazil, the circulation is dominated by northerlies; increasing resolution increases meridional wind variance (Fig. S7). Therefore, we suggest the change in precipitation variance is associated with changes in atmospheric dynamics. A positive feedback exists since an increase in precipitation is associated with a strengthening of local vertical velocity, which strengthens the low-level wind. However, changes in wind variance exhibit a large-scale pattern that suggests changes that are not due solely to local precipitation increases. The variance of the meridional wind increases strongly over the eastern side of the Andes (Fig. S7), highlighting the importance of the orography in modulating the circulation and transporting moisture.

We analyzed the variance of the zonal and meridional components of the moisture flux and found the same patterns as for the low-level wind (not shown), suggesting that changes are mostly attributed to dynamic changes, rather than thermodynamic changes.

5.2 Effects of the Madden-Julian Oscillation

The Madden Julian Oscillation (MJO) strongly affects sub-seasonal precipitation variability over Brazil (Grimm and Silva Dias 1995; Marengo et al. 2008, 2011, 2013; Grimm and Tedeschi 2009; Lewis et al. 2011; Grimm 2019). Therefore, a change in the MJO teleconnection to South America may alter precipitation mean and variance.

Indices of the Madden-Julian Oscillation (MJO) have been computed using NCEP for observed wind and outgoing longwave radiation from NOAA Cooperative Institute for Research in Environmental Sciences data set (Liebmann and Smith 1996), following Wheeler and Hendon (2004), by computing empirical orthogonal functions on daily values of 850 and 200 hPa zonal winds and outgoing longwave radiation. Simulated MJO indices are performed by projecting model data onto the reanalysis EOFs, after first removing the model annual mean and the first three harmonics of the model annual cycle. MJO indices were computed on data first interpolated on a 2.5° resolution. See Wheeler and Hendon (2004) for a longer description of the method. Time series have been deseasonalised and linearly detrended prior to computing impacts of MJO on precipitation mean and variance.

In observations (GPCC), the MJO strongly impacts tropical South American precipitation, leading to above average precipitation during phases 1 and 8, while phases 3, 4 and 5 are associated with anomalously dry conditions (Fig. 6, top two rows), as shown in Grimm (2019). South of 20°S, phases 1, 7 and 8 are associated with anomalously dry conditions and phases 3, 4 and 5 with anomalously wet conditions (Fig. 6, top panel). We select two areas, the Amazon Basin, where differences in precipitation variance between simulations are strong and East Brazil, which is strongly impacted by the MJO. Note the boxes on Fig. 6a. Both areas

351 experience above average precipitation during MJO phases 1, 7 and 8, and below average precipitation
352 during phases 3, 4 and 5 (Fig. 6a-b). HadGEM3 reproduces the impact of MJO on East Brazil and Amazon
353 Basin precipitation in sign and magnitude (Fig. 6i-j). There are no clear differences between N96, N216
354 and N512 simulations, and an impact of the horizontal resolution does not emerge.

355 We show strong impacts of resolution on precipitation variance in Sect. 5.1. Therefore, we address here
356 how precipitation variance could be affected by resolution within each MJO phase. Results are given
357 relative to the variance of the precipitation computed from the full original daily timeseries (with no
358 selection of any specific MJO phases). Results for precipitation variance differ slightly from those for the
359 mean precipitation, with for instance a decrease in the variance during phase 1 when mean precipitation is
360 higher, and stronger during phase 3 when mean precipitation is lower. This difference could also arise from
361 local differences that could strongly impact the area-average. HadGEM3 simulates well the impact of the
362 MJO on the precipitation variance, with above average variance during phases 7 and 8 and below average
363 variance during phases 4 and 5. Unlike the observation, HadGEM3 simulates an increase in the variance of
364 the precipitation during phase 1 of the MJO. N216 and N512 simulations perform better than N96 for phase
365 3 of the MJO, since the N96 simulates reduced precipitation variance while the variance is anomalously
366 high in observation and in the N512 and N216 simulations. However, there is no clear sensitivity of MJO-
367 related precipitation variance to horizontal resolution.

368

369 ## 5.3 Land-atmosphere feedback

370 Soil moisture memory contributes to atmospheric variability and could potentially affect the development
371 of the South American Monsoon System. Land-atmosphere coupling is particularly strong over South
372 America (Koster et al. 2004; Sörensson and Menéndez 2011). In this section we assess the sensitivity of
373 land-atmosphere feedbacks to resolution, using ERA-interim as verifying "observations". The coupling

374 strength metric is defined as the correlation between two variables, weighted by the standard deviation of
375 the reference variable (see Sect. 2.4).

376 Over the Amazon Basin, there is a positive relationship between observed precipitation and observed soil
377 moisture (Fig. 7a), such that an increase in precipitation is associated with anomalously high soil moisture,
378 with soil moisture are coincident with changes in precipitation (Fig. 7e). Over the Amazon Basin and in all
379 HadGEM3 resolutions, the bias in the precipitation—soil moisture coupling strength is small (Fig. 7b-d)
380 and increase in the resolution does not change precipitation—soil moisture coupling strength (Fig. 7i-k;
381 Fig. 7l-n), probably because, over the Amazon, the soil is saturated, such that increases in precipitation
382 variability do not impact soil moisture variability. Soil moisture and evaporation are negatively correlated
383 in observations, such that increased evaporation decreases soil moisture, over the Amazon Basin (Fig. 8a).
384 Over the Amazon Basin, there is not a strong lead-lag relationship between soil moisture and evaporation
385 in observations (Fig. 8e) or in HadGEM3 (Fig, 8f-h). The coupling strength is overestimated in N96 (Fig.
386 8b) but an increase in resolution reduces this overestimation (Fig. 8c-d and Fig.8f-g). Over the Amazon
387 Basin, the moisture budget is energy-limited, rather than moisture limited (Cook et al. 2014). Therefore,
388 we also assessed the coupling strength between temperature and evaporation. An increase in temperature is
389 associated with increased evaporation (Fig. S8) and thus decreased soil moisture, but, in HadGEM3, this
390 coupling strength is not sensitive to resolution (Fig. S8). These results are consistent with our previous
391 results, showing that local recycling plays a moderate role in explaining changes in precipitation variance,
392 which is mainly associated with change in the moisture flux convergence variability (Fig. 6), rather than
393 with a stronger land-atmosphere coupling (Fig. 8).

394 Outside of the Amazon Basin, the soil moisture-precipitation relationship is positive in both observations
395 (Fig. 7a) and HadGEM3 (Fig. 7b-d), with precipitation variability leading soil moisture variability (Fig. 7b
396 and Fig. 7f-h). The increase in soil moisture increases evaporation over eastern Brazil (Fig. 8a). The soil
397 moisture—evaporation coupling strength is too high in all simulations over northeastern and eastern Brazil
398 (Fig. 8b-d), with soil moisture driving evaporation, because evaporation is moisture-limited over northeast

Brazil, with changes in evaporation leading changes in temperature (Fig. S8). The strengths of both precipitation—soil moisture and soil moisture—evaporation couplings are overestimated in N96 (Fig. 7b and Fig.8b) over eastern Brazil and southeastern South America. Increasing resolution reduces this overestimation (Fig. 7cd; Fig. 7i-k; Fig. 8cd; Fig, 8i-k).

5.4 Scales of precipitation

We use the ASoP diagnostics (see section 2.4) to assess daily precipitation features over South America in HadGEM3, and verify them against CMORPH. We compute the fractional contribution to total CMORPH precipitation from four precipitation intensity bins, over South America, with a focus over two sub-regions, the Amazon Basin (AMZ) and southeast South America (SESA). We compare spatial and temporal scales of precipitation features across datasets for the two subregions. Results are given, separately, for light, moderate and heavy rainfall events. We focus on the occurrence and duration of dry spells.

5.4.1 Light precipitation and dry spells

In CMORPH, light precipitation events (<10 mm.day^{-1}) contribute the most of all intensity categories to total precipitation over most of the Andes and northern and southern South America, the Pacific Ocean and western Atlantic Ocean (Fig. 9a). N96 underestimates contributions from light precipitation events over the Andes and southeast Brazil, but overestimates contributions from light precipitation over the Amazon Basin and northeastern Brazil (Fig. 9e). The results are consistent with Seth et al. (2004), which also show an overestimation of the percentage of light rain events over South America. This bias is reduced by increasing resolution to N216 and N512 (Fig, 9i-p; Fig. S9).

Figure 10 shows frequencies of precipitation events, as classified by intensity and duration. Results are shown for two regions: AMZ, where variance is too weak; and SESA, where variance is too high. Over

AMZ and SESA, near-zero precipitation (rainy events of 0.1 – 1 mm.day^{-1}) can last for more than 15 days, while events of 1 – 10 mm.day^{-1} can last for up to 4 or 5 days (Fig. 10a and Fig. 10f). Over AMZ, N96 overestimates the frequency of events of 2 to 12 mm.day^{-1} and underestimates the frequency of those of less than 1 mm.day^{-1}, compared to CMORPH (Fig. 10b). For SESA, N96 underestimates the frequency of precipitation events of less than 1 mm.day^{-1} and lasting between 1 and 8 days; the model overestimates the frequency of near-zero rainy days, lasting more than 8 days (Fig. 10g). Intensity-duration biases improve with resolution over AMZ (Fig. 10c-10d) and SESA (Fig. 10h-10i). However, the biases worsen with resolution for near-zero precipitation lasting for any duration over AMZ, and for intensities between 1-9 mm.day^{-1} with a duration of 1-5 days over SESA.

In addition to events of less than 10 mm.day^{-1}, we assess simulated frequency and duration of dry spells, defined by events of less than 0.1 mm.day^{-1}. We create 2-D histograms for duration versus frequency of dry days over AMZ and SESA (Fig. 11). CMORPH shows more frequent short-duration dry spells as compared to HadGEM3 over AMZ at both native (Fig. 11a) and N96 (Fig. 11c) resolutions. Over SESA, CMORPH also generally shows more frequent dry spells for durations longer than 1 day (Fig. 11b, 11d). The sensitivity of dry-spell frequency to model resolution is generally smaller than the model bias. Once all datasets are interpolated to the common N96 resolution, N96 produces longer and more frequent dry spells than N216 and N512, and is closer to CMORPH.

5.4.2 Moderate precipitation

Over most other parts of South America (i.e. Amazon and central and eastern Brazil), most of the total precipitation is contributed by light to moderate events (10-40 mm.day^{-1}; Fig. 9a-c). Compared to CMORPH, N96 overestimates the contribution from moderate events, to total precipitation, over the Andes and underestimates this contribution over South America outside of the Andes (Fig. 9f, 9g). Although the spatial pattern of biases is similar to N96, biases in contribution from moderate rainfall to total precipitation reduce when increasing resolution (Fig. 9f-j-n and Fig. 9g-k-o; Fig. S9).

Over AMZ and SESA, most precipitation comes from moderate events in both CMORPH and HadGEM3 (Fig. 10b-e). Over AMZ, CMORPH distribution peaks at ~30 mm.day^{-1} (Fig. 10b, 10d), when using the CMORPH native grid (Fig. 10b), and at ~20 mm.day^{-1} when using the N96 grid (Fig. 10d). At their native resolutions, N96, N216 and N512 have a primary peak at ~9 mm.day^{-1} and a secondary peak at ~30 mm.day^{-1} (Fig. 10b). On the N96 grid, the secondary peak is removed in N216 and N512. As the fractional contribution in HadGEM3 peaks at lower intensities for all three resolutions, HadGEM3 overestimates the contribution from intensities below ~15 mm.day^{-1} and underestimates contribution from intensities above 15 mm.day^{-1} (Fig. 10b). When compared on their native grids, the model biases reduce with resolution over AMZ. However, once interpolated to N96, N512 has the largest bias in fractional contribution, around the peak intensity (i.e. at ~10 mm.day^{-1}). Over AMZ, N96 underestimates the frequency of events of 12-40 mm.day^{-1} (Fig. 10d and Fig. 12b). Increasing resolution reduces the biases for the frequency of events of 12-25 mm.day^{-1} but leads to an underestimation of precipitation of 30 to 40 mm.day^{-1} (Fig. 10b and Fig. 12c-e). Over SESA, distribution peaks at ~20-30 mm.day^{-1} (Fig. 12c and Fig. 12e). Over SESA, N96 underestimates (overestimates) the frequency of events of 2-20 mm.day^{-1} (20-40 mm.day^{-1}) (Fig. 10g; Fig. 12e). These biases are reduced in at N216 and N512 (Fig. 10h-j; Fig. 12e).

5.4.3 Heavy precipitation

Parts of the Peruvian Andes, Uruguay and northeastern Argentina receive most of their rainfall from heavy events (>40 mm.day^{-1}; Fig. 9d). N96 overestimates these contributions (>40 mm.day^{-1}) over central Brazil, the eastern Amazon and southeastern Brazil (Fig. 9h). Like for the light and moderate events, increasing resolution reduces these biases (Fig. 9h-p and Fig. S9). This suggests that, at higher resolution, HadGEM3 performs better for the frequency of extreme events, such as those that lead to flooding. However, the improvements primarily come from the increase from N96 to N216, not from N216 to N512 (Fig. S9). In addition, N96 overestimates the frequency of events > 40 mm.day^{-1} over AMZ and SESA (Fig. 10b; Fig. 10g). Increasing resolution reduces these biases, again mostly due to increase from the N96 to N216

resolution, not from N216 to N512. For AMZ, N512 has a higher bias than N216 for events of 40-90 mm.day^{-1}.

5.4.4 Temporal and spatial scales

To compare spatial and temporal scales of precipitation features across datasets, we plot correlations as functions of distance (Fig. 13a-d) and time (Fig. 13e-h) (see section 2.4). Over AMZ, N96 overestimates the spatial and temporal scales of precipitation events relative to CMORPH, on their native grids (Fig. 13a and Fig. 13e). However, once CMORPH is interpolated to the N96 grid, N96 simulation underestimates the spatial scale (and overestimates the temporal scale) of precipitation (Fig 13b and Fig. 13f), highlighting that results strongly depend on the analysis grid. For SESA, N96 also underestimates the spatial scale and overestimates temporal scale of precipitation (Fig. 13d-g-h). When considering native grids only, there are no clear differences between N96 and CMORPH for the spatial extent of precipitation events (Fig. 13c).

On native grids, N96 simulates events with larger spatial scales than N216 and N512 (Fig. 13a). However, this is mainly due to the coarse N96 grid. While all datasets are interpolated onto the N96 grid, N96 events are smaller than those in N216 and N512, which show similar scales and are closer to CMORPH (Fig. 13b). Over SESA, spatial scales are similar in all simulations, on their native grids (Fig. 13c). However, as for AMZ, at N96 resolution N512 and N216 are closer to CMORPH than to N96 (Fig. 13d). For both AMZ and SESA, therefore, the spatial features of daily precipitation events are better simulated at higher resolution.

At all resolutions, simulated precipitation features persist longer than in CMORPH (Fig. 13e-h). Over AMZ and SESA, biases are lowest in N96, which simulates events that are less persistent than in N216 and N512 (Fig. 13f, Fig. 13h). This bias increases at higher resolution. Therefore, increasing horizontal resolution does not improve biases in temporal scales of precipitation.

6 Conclusion

We assess the effects of increasing horizontal resolution on simulated South American precipitation. We use atmosphere-only simulations, performed with HadGEM3-GC3.1 (Williams et al. 2018) at three horizontal resolutions: N96 (~130 km, 1.88° x 1.25), N216 (~60 km, 0.83° × 0.56°), and N512 (~25 km, 0.35° x 0.23°). We assess, systematically, how the step change between each resolution effects simulated precipitation, focusing on precipitation mean and variance, and on fine scale processes, such as temporal and spatial scales, frequency of heavy and light precipitation events and dry-spell durations.

We show that the atmosphere-only simulations have systematic biases in simulating annual mean and seasonal mean precipitation over South America. Northeast Brazil is anomalously dry, while the southeast Brazil and the Andes are too wet. These biases are mostly due to atmospheric circulation biases: underestimated trade easterlies, and a displaced anticyclonic circulation over southeast Brazil, both acting to modify moisture transport over South America. Increasing horizontal resolution affects the simulated precipitation. For instance, precipitation biases reduce over the Andes and over northeast Brazil. It is worth increasing the resolution to N512 (~25 km) for simulating precipitation over the Andes Mountains. This is consistent with Vannière et al. (2019), which shows that the added value of increasing horizontal resolution is greatest over orography. Over northeast Brazil, the largest improvement comes from increasing resolution to N216 (~60 km); a further increase to N512 is only associated with moderate changes. Increasing resolution does not improve model biases over the Amazon Basin. These results are consistent with Roberts et al. (2018) for the Amazon Basin and northeast and south Brazil. In addition, improvements vary seasonally: changes are the strongest over northeast Brazil in DJF and MAM, when precipitation is also highest. Over the Andes, the results are similar in all seasons.

Biases in mean precipitation are collocated with biases in regional precipitation variance. For instance, northeast Brazil is too dry and HadGEM3-GC3.1 systematically underestimates precipitation variance,

525 while southeast Brazil is too wet and HadGEM3-GC3.1 systematically overestimates precipitation
526 variance. However, this does not hold for the Amazon Basin, which is too wet but where the precipitation
527 variance is strongly underestimated. Precipitation variance is stronger at daily scales than at monthly scales;
528 biases are strongest in DJF and over the Amazon Basin. Increasing resolution increases precipitation
529 variance, hence reducing biases. The increase in precipitation variance is associated with an increase in
530 moisture flux convergence variance over land, and with changes in the variance of the low-level winds;
531 local recycling of evaporation has a limited role. Relatedly, coupling strengths between evaporation, soil
532 moisture and precipitation are only weakly sensitive to resolution, except for some improvements in
533 coupling strength over eastern and southeastern Brazil. We found only modest sensitivity to resolution for
534 the teleconnections of the El-Niño Southern Oscillation and Madden-Julian Oscillation to land
535 precipitation. This suggests that changes in precipitation mean and variance are not due to changes in these
536 teleconnections.
537
538 HadGEM3-GC3.1 has biases in its precipitation distribution. For instance, the model does not produce
539 enough dry days over the Amazon Basin or moderate rain days (10-40 $mm.day^{-1}$), while simulating too
540 many light events (<10 $mm.day^{-1}$) and heavy events (>40 $mm.day^{-1}$). Over southeast Brazil, the model
541 simulates too few short dry spells and too many long ones. HadGEM3-GC3.1 simulates too few and too
542 short events of 2 to 16 $mm.day^{-1}$, but simulates too many and too long events of more than 20 $mm.day^{-1}$.
543 These metrics are important for understanding the ability of climate models to simulate high-impact events.
544 Increasing resolution reduces these biases; N512 is therefore better at simulating precipitation distributions
545 than N96. In addition, increasing the horizontal resolution increases the spatial scale of daily rain events,
546 suggesting a better simulation of organised mesoscale systems. However, the persistence of precipitation
547 events is better simulated at N96, showing no clear sensitivity to resolution. Other models also overestimate
548 light events at the expense of heavy events over the Amazon and eastern Brazil, and overestimate heavy
549 events at the expense of lighter ones in southeast Brazil (Seth et al. 2004).
550

551 Over South America, precipitation results from the combination of the predominant role played by the
552 InterTropical Convergence Zone and the South Atlantic Convergence Zone (Waliser et al. 1993; Liebmann
553 et al. 1999). In addition, mesoscale systems such as squall lines may be responsible for a large fraction of
554 Amazonian precipitation (Cohen et al. 1995). Our results show that increasing the horizontal resolution
555 increases the spatial scale of rain events, i.e. of the mesoscale systems, over both Amazonia and southeast
556 Brazil. Therefore, we speculate that increasing resolution could lead to more organized convective systems,
557 which would be consistent with the increase in moisture flux convergence, as shown over South America
558 at the highest resolution. This would be consistent with Vellinga et al. (2016) who showed that N512
559 resolution improved mesoscale systems over West Africa relative to N96 or N216. Conversely, the decrease
560 in the persistence of such events (highest at the N96 resolution) could be associated with an increase in
561 daily rainfall variability, because of less persistent rainy events. Those are hypotheses that should be
562 assessed in more detail in a specific study, potentially with models at sufficiently high resolution to disable
563 convective parameterisations.
564
565 Although we hypothesized that increasing resolution might affect the ability of climate models to predict
566 precipitation, Bombardi et al. (2018) have shown that an improvement of South American precipitation
567 prediction due to an increase in resolution is not straightforward. In addition to resolution, further works
568 should, therefore, be devoted to understanding the effects of physic, on prediction system performance.
569
570 The mechanism for increases in precipitation variance with resolution are still unclear. The increase in
571 precipitation variance is a global feature, not limited to South America (Fig. S10). Further work is needed
572 to understand better this behavior at global scale. Besides, we used AMIP-type simulations; and results
573 could be different in coupled models, in which the ocean can interact with atmospheric variability,
574 particularly when accounting for SST teleconnections.
575
576

Code availability. Codes used to perform analysis and figures are publicly available at https://doi.org/10.5281/zenodo.3840095. For the analysis of the scales of precipitation (ASoP), codes are available on https://github.com/nick-klingaman/dubstep/tree/master/asop and https://github.com/nick-klingaman/dubstep/tree/master/asop_duration.

Data availability. The model data used in the analysis are available from the CMIP6 Earth System Grid Federation, for N96 (HadGEM3-GC31-LM; https://doi.org/ 10.22033/ESGF/CMIP6.1321), N216 (HadGEM3-GC31-MM; https://doi.org/ 10.22033/ESGF/CMIP6.1902) and N512 (HadGEM3-GC31-HM; https://doi.org/ 10.22033/ESGF/CMIP6.446). The list of persistent identifiers of the data we have used is available at **https://doi.org/10.5281/zenodo.3840095**

Author contributions. AC, PAM and PC performed the data analysis. PAM prepared the manuscript with contributions from all co-authors.

Acknowledgements

This work was supported by the Newton Fund through the Met Office Climate Science for Service Partnership Brazil (CSSP Brazil). NPK was funded by an Independent Research Fellowship from the Natural Environment Research Council (NE/L010976/1) and by the NERC/GCRF programme Atmospheric hazard in developing countries: risk assessment and early warnings (ACREW). Detailed calculations and code for the ASoP diagnostics are available at https://github.com/achevuturi/asop_duration. NOAA OLR data can be obtained from the website (https://www.esrl.noaa.gov/psd/data/gridded/data.interp_OLR.html). Authors thank Dr. Pier Luigi Vidale for his insightful and constructive comments. The authors thank the two anonymous reviewers for their constructive comments and suggestions.

608 **References**

609 Bacmeister JT, Wehner MF, Neale RB, et al (2013) Exploratory High-Resolution Climate Simulations
610 using the Community Atmosphere Model (CAM). J Clim 27:3073–3099. doi: 10.1175/JCLI-D-13-
611 00387.1

612 Bombardi RJ, Carvalho LM V (2008) IPCC global coupled model simulations of the South America
613 monsoon system. Clim Dyn 33:893. doi: 10.1007/s00382-008-0488-1

614 Bombardi RJ, Trenary L, Pegion, K, Cash, B, DelSole, T, Kinter JL (2018). Seasonal predictability of
615 summer rainfall over South America. J Clim 31(20): 8181-8195. doi.org/10.1175/JCLI-D-18-0191.1.

616 Coelho CAS, de Oliveira CP, Ambrizzi T, et al (2016) The 2014 southeast Brazil austral summer drought:
617 regional scale mechanisms and teleconnections. Clim Dyn 46:3737–3752. doi: 10.1007/s00382-015-
618 2800-1

619 Cohen JCP, Silva Dias MAF, Nobre CA (1995) Environmental Conditions Associated with Amazonian
620 Squall Lines: A Case Study. Mon Weather Rev 123:3163–3174. doi: 10.1175/1520-
621 0493(1995)123<3163:ECAWAS>2.0.CO;2

622 Cook BI, Smerdon JE, Seager R, Coats S (2014) Global warming and 21st century drying. Clim Dyn
623 43:2607–2627. doi: 10.1007/s00382-014-2075-y

624 Custodio M de S, da Rocha RP, Ambrizzi T, et al (2017) Impact of increased horizontal resolution in
625 coupled and atmosphere-only models of the HadGEM1 family upon the climate patterns of South
626 America. Clim Dyn 48:3341–3364. doi: 10.1007/s00382-016-3271-8

627 Custódio M de S, Porfírio da Rocha R, Vidale PL (2012) Analysis of precipitation climatology simulated
628 by high resolution coupled global models over the South America. Hydrol Res Lett 6:92–97. doi:
629 10.3178/hrl.6.92

630 Dai A (2006) Precipitation Characteristics in Eighteen Coupled Climate Models. J Clim 19:4605–4630.
631 doi: 10.1175/JCLI3884.1

632 De Sales F, Xue Y (2011) Assessing the dynamic-downscaling ability over South America using the
633 intensity-scale verification technique. Int J Climatol 31:1205–1221. doi: 10.1002/joc.2139

634 Dee DP, Uppala SM, Simmons AJ, et al (2011) The ERA-Interim reanalysis: configuration and
635 performance of the data assimilation system. Q J R Meteorol Soc 137:553–597. doi: 10.1002/qj.828

636 DelSole T, Shukla J (2010) Model Fidelity versus Skill in Seasonal Forecasting. J Clim 23:4794–4806.
637 doi: 10.1175/2010JCLI3164.1

638 Delworth TL, Rosati A, Anderson W, et al (2011) Simulated Climate and Climate Change in the GFDL
639 CM2.5 High-Resolution Coupled Climate Model. J Clim 25:2755–2781. doi: 10.1175/JCLI-D-11-
640 00316.1

641 Demory M-E, Vidale PL, Roberts MJ, et al (2014) The role of horizontal resolution in simulating drivers
642 of the global hydrological cycle. Clim Dyn 42:2201–2225. doi: 10.1007/s00382-013-1924-4

643 Doblas-Reyes FJ, Andreu-Burillo I, Chikamoto Y, et al (2013) Initialized near-term regional climate
644 change prediction. Nat Commun 4:1715. doi: 10.1038/ncomms2704

645 Falco M, Carril AF, Menéndez CG, et al (2019) Assessment of CORDEX simulations over South
646 America: added value on seasonal climatology and resolution considerations. Clim Dyn 52:4771–
647 4786. doi: 10.1007/s00382-018-4412-z

648 Gent PR, Yeager SG, Neale RB, et al (2010) Improvements in a half degree atmosphere/land version of
649 the CCSM. Clim Dyn 34:819–833. doi: 10.1007/s00382-009-0614-8

650 Grimm AM (2019) Madden--Julian Oscillation impacts on South American summer monsoon season:
651 precipitation anomalies, extreme events, teleconnections, and role in the MJO cycle. Clim Dyn. doi:
652 10.1007/s00382-019-04622-6

653 Grimm AM, Silva Dias PL (1995) Analysis of Tropical–Extratropical Interactions with Influence
654 Functions of a Barotropic Model. J Atmos Sci 52:3538–3555. doi: 10.1175/1520-
655 0469(1995)052<3538:AOTIWI>2.0.CO;2

656 Grimm AM, Tedeschi RG (2009) ENSO and Extreme Rainfall Events in South America. J Clim 22:1589–
657 1609. doi: 10.1175/2008JCLI2429.1

658 Haarsma RJ, Roberts MJ, Vidale PL, et al (2016) High resolution model intercomparison project
659 (HighResMIP v1. 0) for CMIP6. Geosci Model Dev 9:4185–4208

660 Jia L, Yang X, Vecchi GA, et al (2014) Improved Seasonal Prediction of Temperature and Precipitation
661 over Land in a High-Resolution GFDL Climate Model. J Clim 28:2044–2062. doi: 10.1175/JCLI-D-
662 14-00112.1

663 Joyce RJ, Janowiak JE, Arkin PA, Xie P (2004) CMORPH: A Method that Produces Global Precipitation
664 Estimates from Passive Microwave and Infrared Data at High Spatial and Temporal Resolution. J
665 Hydrometeorol 5:487–503. doi: 10.1175/1525-7541(2004)005<0487:CAMTPG>2.0.CO;2

666 Jung T, Miller MJ, Palmer TN, et al (2011) High-Resolution Global Climate Simulations with the
667 ECMWF Model in Project Athena: Experimental Design, Model Climate, and Seasonal Forecast
668 Skill. J Clim 25:3155–3172. doi: 10.1175/JCLI-D-11-00265.1

669 Kanamitsu M, Ebisuzaki W, Woollen J, et al (2002) NCEP–DOE AMIP-II Reanalysis (R-2). Bull Am
670 Meteorol Soc 83:1631–1643. doi: 10.1175/BAMS-83-11-1631

671 Kirtman BP, Bitz C, Bryan F, et al (2012) Impact of ocean model resolution on CCSM climate
672 simulations. Clim Dyn 39:1303–1328. doi: 10.1007/s00382-012-1500-3

673 Klingaman NP, Martin GM, Moise A (2017) ASoP (v1.0): a set of methods for analyzing scales of
674 precipitation in general circulation models. Geosci Model Dev 10:57–83. doi: 10.5194/gmd-10-57-
675 2017

676 Knight JR, Folland CK, Scaife AA (2006) Climate impacts of the Atlantic Multidecadal Oscillation.
677 Geophys Res Lett 33:L17706. doi: 10.1029/2006GL026242

678 Koster RD, Dirmeyer PA, Guo Z, et al (2004) Regions of Strong Coupling Between Soil Moisture and
679 Precipitation. Science (80-) 305:1138 LP – 1140. doi: 10.1126/science.1100217

680 Koutroulis AG, Grillakis MG, Tsanis IK, Papadimitriou L (2016) Evaluation of precipitation and
681 temperature simulation performance of the CMIP3 and CMIP5 historical experiments. Clim Dyn

682 47:1881–1898. doi: 10.1007/s00382-015-2938-x

683 Lewis SL, Brando PM, Phillips OL, et al (2011) The 2010 Amazon Drought. Science (80-) 331:554 LP –
684 554. doi: 10.1126/science.1200807

685 Liebmann B, Kiladis GN, Marengo J, et al (1999) Submonthly Convective Variability over South
686 America and the South Atlantic Convergence Zone. J Clim 12:1877–1891. doi: 10.1175/1520-
687 0442(1999)012<1877:SCVOSA>2.0.CO;2

688 Liebmann B, Smith CA (1996) Description of a Complete (Interpolated) Outgoing Longwave Radiation
689 Dataset. Bull Am Meteorol Soc 77:1275–1277

690 Liu WT, Juárez RIN (2001) ENSO drought onset prediction in northeast Brazil using NDVI. Int J Remote
691 Sens 22:3483–3501. doi: 10.1080/01431160010006430

692 Marengo JA, Alves LM, Soares WR, et al (2013) Two Contrasting Severe Seasonal Extremes in Tropical
693 South America in 2012: Flood in Amazonia and Drought in Northeast Brazil. J Clim 26:9137–9154.
694 doi: 10.1175/JCLI-D-12-00642.1

695 Marengo JA, Nobre CA, Tomasella J, et al (2008) The Drought of Amazonia in 2005. J Clim 21:495–
696 516. doi: 10.1175/2007JCLI1600.1

697 Marengo JA, Tomasella J, Alves LM, et al (2011) The drought of 2010 in the context of historical
698 droughts in the Amazon region. Geophys Res Lett 38:. doi: doi:10.1029/2011GL047436

699 Martin GM, Klingaman NP, Moise AF (2017) Connecting spatial and temporal scales of tropical
700 precipitation in observations and the MetUM-GA6. Geosci Model Dev 10:105–126. doi:
701 10.5194/gmd-10-105-2017

702 McClean JL, Bader DC, Bryan FO, et al (2011) A prototype two-decade fully-coupled fine-resolution
703 CCSM simulation. Ocean Model 39:10–30. doi: https://doi.org/10.1016/j.ocemod.2011.02.011

704 Power S, Casey T, Folland C, et al (1999) Inter-decadal modulation of the impact of ENSO on Australia.
705 Clim Dyn 15:319–324. doi: 10.1007/s003820050284

706 Rayner NA, Brohan P, Parker DE, et al (2006) Improved Analyses of Changes and Uncertainties in Sea
707 Surface Temperature Measured In Situ since the Mid-Nineteenth Century: The HadSST2 Dataset. J
708 Clim 19:446–469. doi: 10.1175/JCLI3637.1

709 Roberts MJ, Baker A, Blockley EW, et al (2019) Description of the resolution hierarchy of the global
710 coupled HadGEM3-GC3.1 model as used in CMIP6 HighResMIP experiments. Geosci Model Dev
711 12:4999–5028. doi: 10.5194/gmd-12-4999-2019

712 Roberts MJ, Vidale PL, Senior C, et al (2018) The Benefits of Global High Resolution for Climate
713 Simulation: Process Understanding and the Enabling of Stakeholder Decisions at the Regional
714 Scale. Bull Am Meteorol Soc 99:2341–2359. doi: 10.1175/BAMS-D-15-00320.1

715 Sakamoto TT, Komuro Y, Nishimura T, et al (2012) MIROC4h—a new high-resolution atmosphere-
716 ocean coupled general circulation model. J Meteorol Soc Japan Ser II 90:325–359

717 Schneider U, Becker A, Finger P, et al (2014) GPCC's new land surface precipitation climatology based

718 on quality-controlled in situ data and its role in quantifying the global water cycle. Theor Appl
719 Climatol 115:15–40. doi: 10.1007/s00704-013-0860-x

720 Seth A, Rojas M, Liebmann B, Qian J-H (2004) Daily rainfall analysis for South America from a regional
721 climate model and station observations. Geophys Res Lett 31:. doi: 10.1029/2003GL019220

722 Shaffrey LC, Stevens I, Norton WA, et al (2009) U.K. HiGEM: The New U.K. High-Resolution Global
723 Environment Model—Model Description and Basic Evaluation. J Clim 22:1861–1896. doi:
724 10.1175/2008JCLI2508.1

725 Sierra JP, Arias PA, Vieira SC (2015) Precipitation over northern South America and its seasonal
726 variability as simulated by the CMIP5 models. Adv Meteorol 2015:

727 Small RJ, Bacmeister J, Bailey D, et al (2014) A new synoptic scale resolving global climate simulation
728 using the Community Earth System Model. J Adv Model Earth Syst 6:1065–1094. doi:
729 doi:10.1002/2014MS000363

730 Solman SA, Blázquez J (2019) Multiscale precipitation variability over South America: Analysis of the
731 added value of CORDEX RCM simulations. Clim Dyn 53:1547–1565. doi: 10.1007/s00382-019-
732 04689-1

733 Sörensson AA, Menéndez CG (2011) Summer soil—precipitation coupling in South America. Tellus A
734 Dyn Meteorol Oceanogr 63:56–68. doi: 10.1111/j.1600-0870.2010.00468.x

735 Sun Y, Solomon S, Dai A, Portmann RW (2006) How Often Does It Rain? J Clim 19:916–934. doi:
736 10.1175/JCLI3672.1

737 Trenberth KE (2011) Changes in precipitation with climate change. Clim Res 47:123–138

738 Vannière B, Demory M-E, Vidale PL, et al (2019) Multi-model evaluation of the sensitivity of the global
739 energy budget and hydrological cycle to resolution. Clim Dyn 52:6817–6846. doi: 10.1007/s00382-
740 018-4547-y

741 Vellinga M, Roberts M, Vidale PL, et al (2016) Sahel decadal rainfall variability and the role of model
742 horizontal resolution. Geophys Res Lett 43:326–333. doi: 10.1002/2015GL066690

743 Vera C, Higgins W, Amador J, et al (2006) Toward a Unified View of the American Monsoon Systems. J
744 Clim 19:4977–5000. doi: 10.1175/JCLI3896.1

745 Villamayor J, Ambrizzi T, Mohino E (2018) Influence of decadal sea surface temperature variability on
746 northern Brazil rainfall in CMIP5 simulations. Clim Dyn 51:563–579. doi: 10.1007/s00382-017-
747 3941-1

748 Waliser DE, Graham NE, Gautier C (1993) Comparison of the Highly Reflective Cloud and Outgoing
749 Longwave Radiation Datasets for Use in Estimating Tropical Deep Convection. J Clim 6:331–353.
750 doi: 10.1175/1520-0442(1993)006<0331:COTHRC>2.0.CO;2

751 Walters D, Baran AJ, Boutle I, et al (2019) The Met Office Unified Model Global Atmosphere 7.0/7.1
752 and JULES Global Land 7.0 configurations. Geosci Model Dev 12:1909–1963. doi: 10.5194/gmd-
753 12-1909-2019

754 Wei J, Dirmeyer PA (2012) Dissecting soil moisture-precipitation coupling. Geophys Res Lett 39:. doi:
755 10.1029/2012GL053038

756 Wheeler MC, Hendon HH (2004) An All-Season Real-Time Multivariate MJO Index: Development of an
757 Index for Monitoring and Prediction. Mon Weather Rev 132:1917–1932. doi: 10.1175/1520-
758 0493(2004)132<1917:AARMMI>2.0.CO;2

759 Williams KD, Copsey D, Blockley EW, et al (2018) The Met Office Global Coupled Model 3.0 and 3.1
760 (GC3.0 and GC3.1) Configurations. J Adv Model Earth Syst 10:357–380. doi:
761 doi:10.1002/2017MS001115

762 Willmott CJ, Matsuura K, Legates DR (2001) Terrestrial air temperature and precipitation: monthly and
763 annual time series (1950–1999). Cent Clim Res version 1:

764 Yin L, Fu R, Shevliakova E, Dickinson RE (2013) How well can CMIP5 simulate precipitation and its
765 controlling processes over tropical South America? Clim Dyn 41:3127–3143. doi: 10.1007/s00382-
766 012-1582-y

767 Zeng N, Yoon J-H, Marengo JA, et al (2008) Causes and impacts of the 2005 Amazon drought. Environ
768 Res Lett 3:14002. doi: 10.1088/1748-9326/3/1/014002

769

770

771

772

773

774

775

776

777

778

779

780

781

782

783

Figures

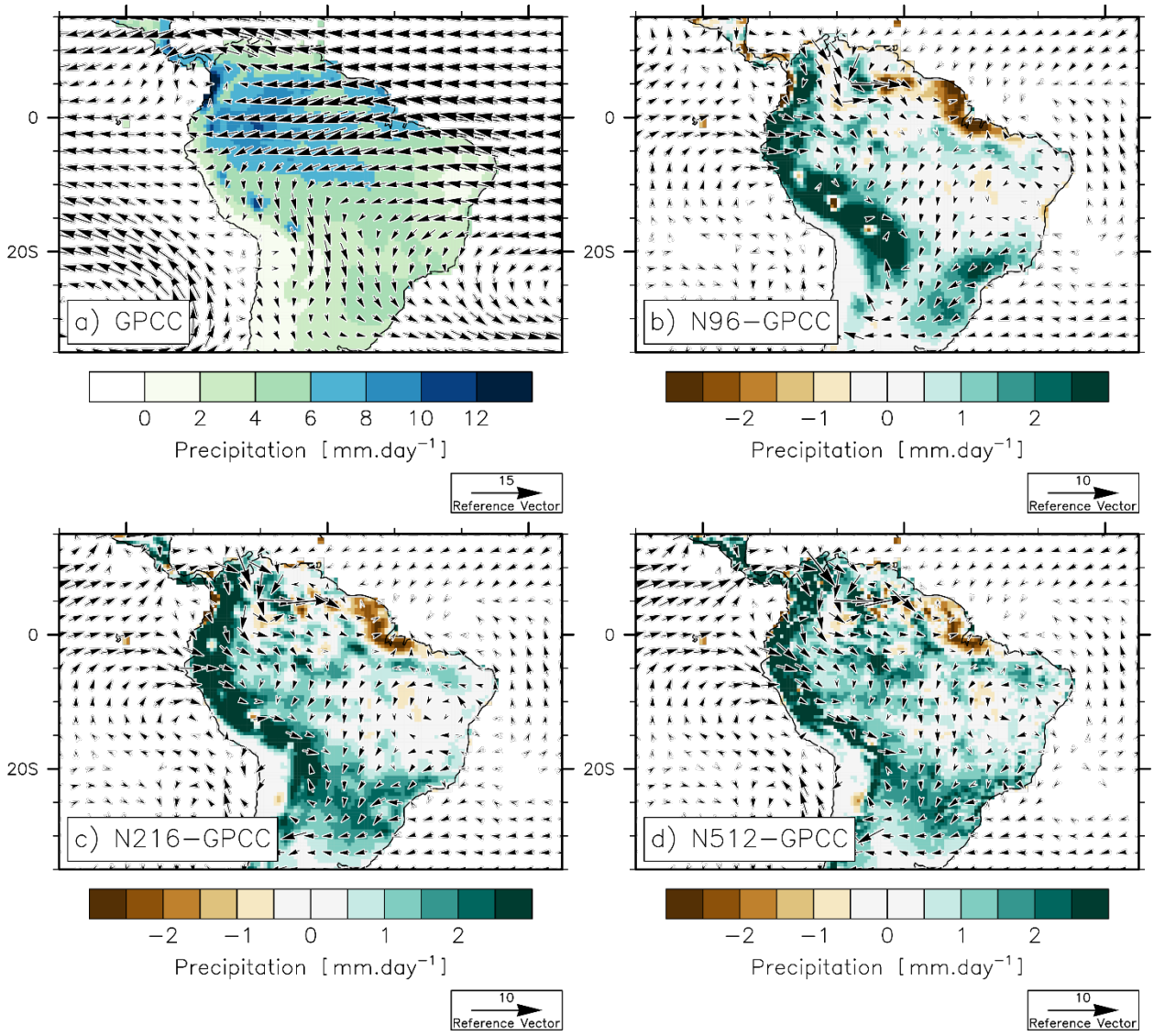

Figure 1: (a) Observed mean annual precipitation (GPCC; mm.day^{-1}; colors) and 850 hPa wind (NCEP; m.s^{-1}; vectors), averaged over the period 1950-2014. Bias in precipitation and 850 hPa wind in (b) N96 (i.e. N96-GPCC), (c) N216 (i.e. N216-GPCC) and (d) N512 (i.e. N512-GPCC). On the panels (a), (b) and (c) biases in precipitation are shown when statistically significant in all of the three members, according to a Student's t-test and a 95% confidence level.

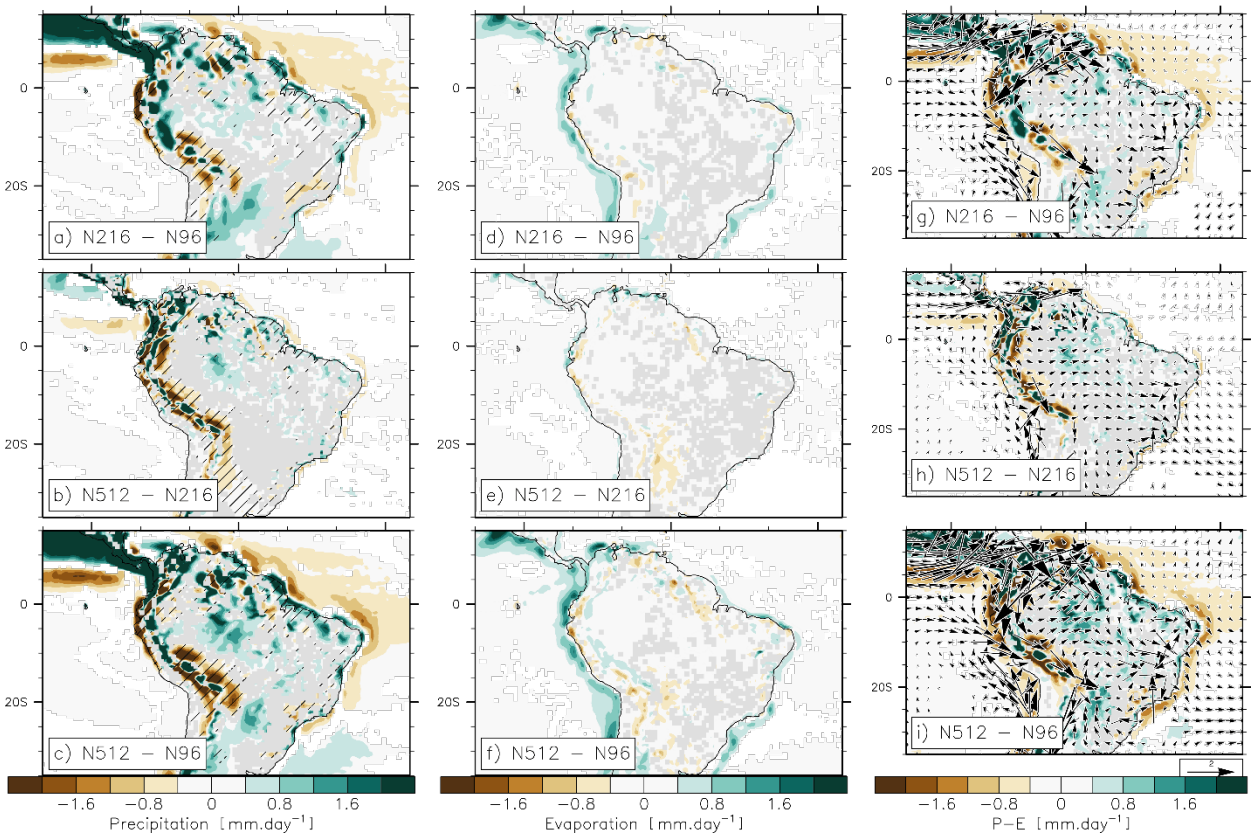

Figure 2: Ensemble-mean (a) N216-N96, (b) N512-N216 and (c) N512-N96 differences in mean annual precipitation (mm.day^{-1}). (d), (e) and (f): same as (a), (b) and (c) but for evaporation (mm.day^{-1}). (g), (h) and (i): same as (a), (b) and (c) but for the moisture flux convergence (P-E; mm.day^{-1}; colors) and the 850 hPa wind (m.s^{-1}; vectors). For precipitation (i.e. left row) stippling indicates that the mean bias is reduced at the higher than at the lower horizontal resolution. Differences are shown when significantly different to zero according to a Student's t-test and a 95% confidence level.

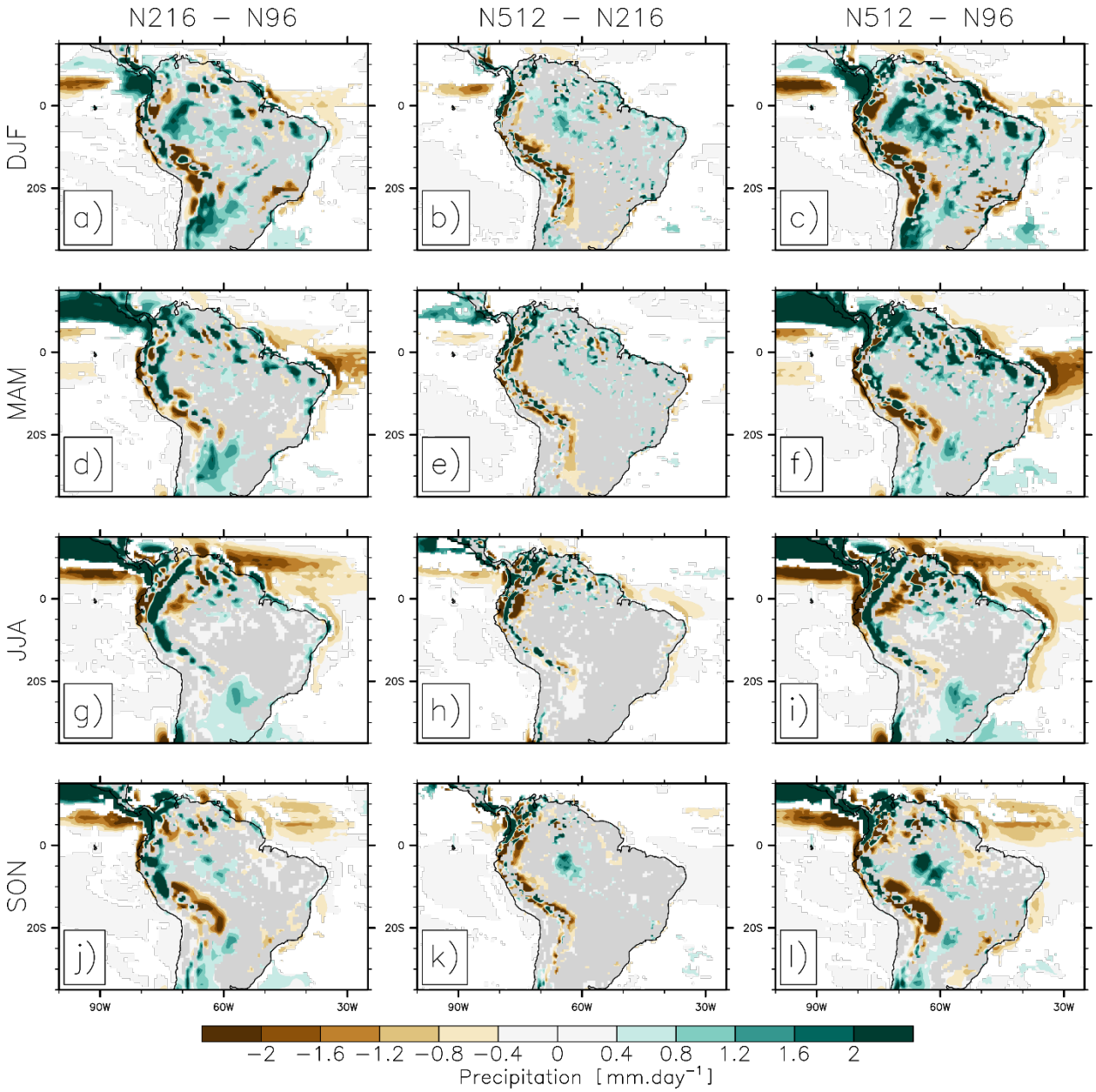

Figure 3: Ensemble-mean N216-N96 difference in (a) DJF, (d), MAM, (g) JJA and (j) SON precipitation ($mm.day^{-1}$). (b), (e), (h) and (k), as in (a), (d), (g) and (j) but for N512-N216. (c), (f), (i) and (l), as in (a), (d), (g) and (j) but for N512-N96. Differences are shown when statistically different to zero, according to a Student's t-test and a 95% confidence level.

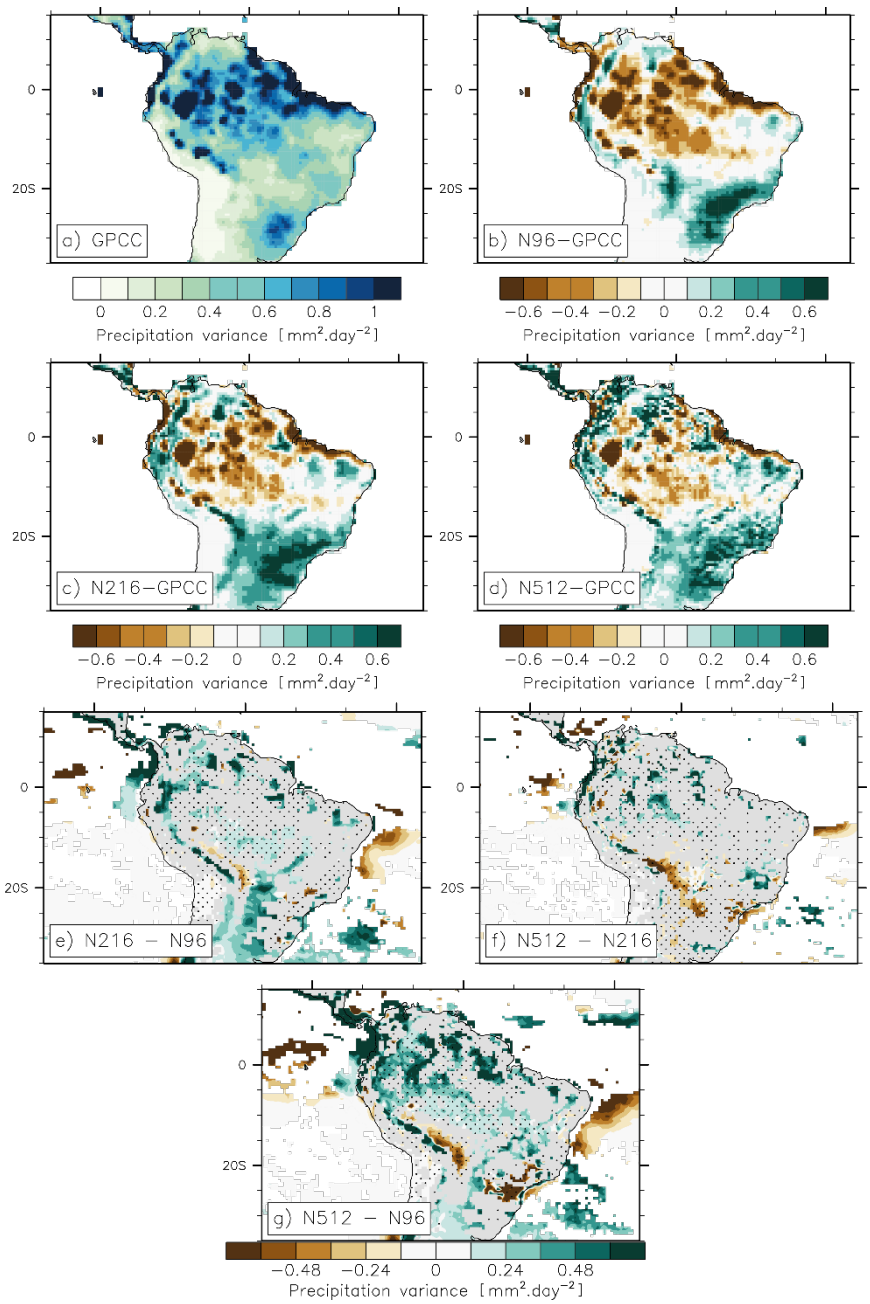

Figure 4: (a) Observed annual-mean precipitation variance (GPCC; $mm^2.day^{-2}$), as computed over the period 1982-2014. A linear trend is removed. Bias in annual-mean precipitation variance in (b) N96 (i.e. N96-GPCC), (c) N216 (i.e. N216-GPCC) and (d) N512 (i.e. N512-GPCC). (e) N216-N96, (f) N512-N216 and (g) N512-N96 differences in annual-mean precipitation variance. On (b), (c) and (d), biases are shown when all three members produces a bias that is significant according to a f-test and a 95% confidence level. On (e), (f) and (g), stippling indicates that the bias is improved at the higher than at the lower resolution.

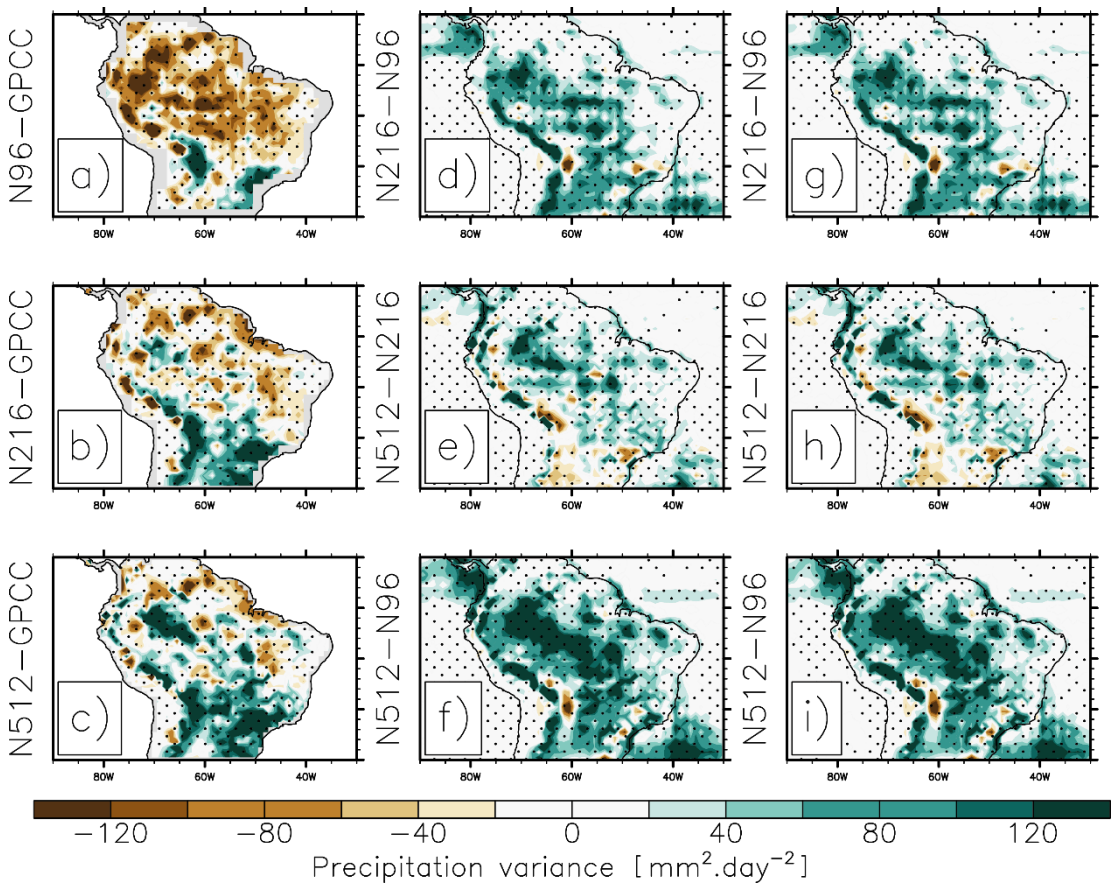

Figure 5: (Left row) Bias in daily precipitation variance ($mm^2.day^{-2}$) for (a) N96 (i.e. N96-GPCC), (b) N216 (i.e. N216-GPCC) and (b) N512 (i.e. N512-GPCC) simulations, over the DJF period. Seasonal cycle and linear trend are removed prior to computing variance. Differences in daily precipitation variance ($mm^2.day^{-2}$) for (d) N216-N96, (e) N512-N216 and (f) N512-N96. (g), (h) and (i), as in (d), (e) and (f) but for P-E (precipitation minus evaporation) variance.

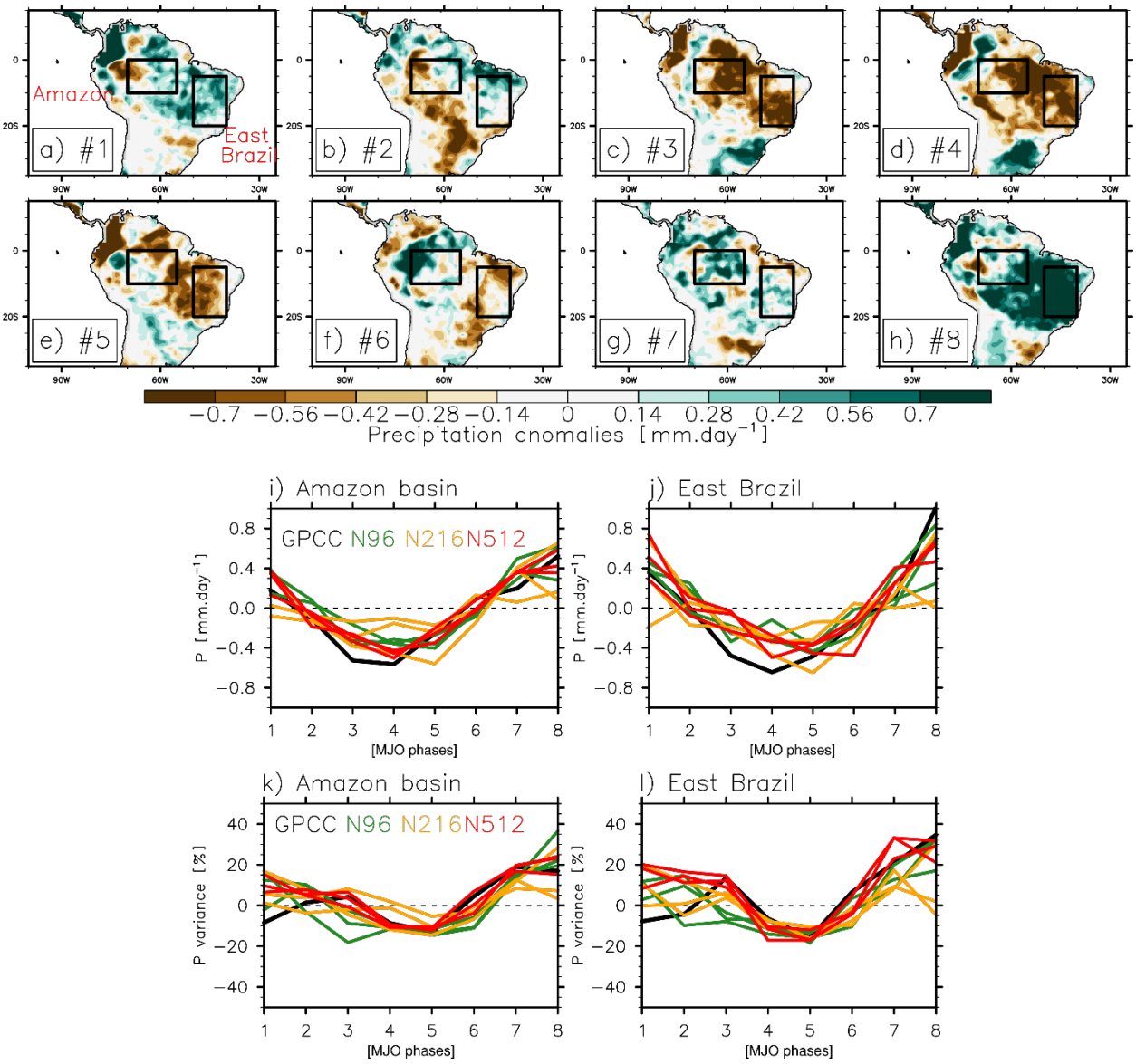

Figure 6: Observed impacts of Madden-Julian Oscillation phase (a) 1, (b) 2, (c) 3, (d) 4, (e) 5, (f) 6, (g) 7 and (h) 8 on precipitation (GPCC and NCEP for the RMM index; mm.day^{-1}). Precipitation anomalies (mm.day^{-1}), associated with each phase of the Madden-Julian Oscillation, relative to the period 1982-2014, and averaged over the (i) Amazon Basin and (j) East Brazil (see the box on (a)), for observation (black), N96 (green), N216 (orange) and N512 (red). (k) and (l), as in (i) and (j) but for precipitation variance, in percent (%) of the precipitation variance over the period 1982-2014.

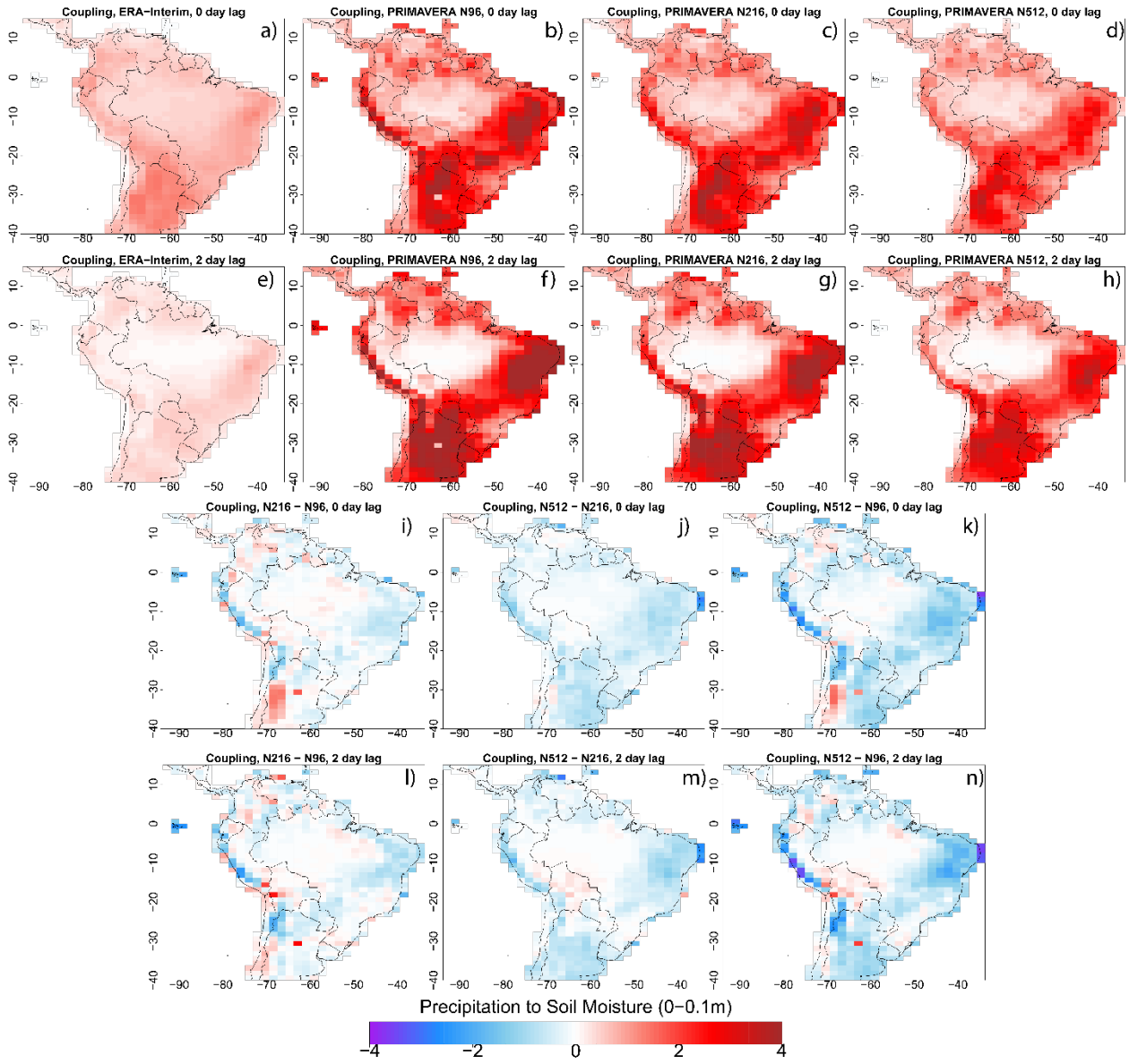

841

842 Figure 7: (a) Observed (ERA-Interim) and (b) N96, (c) N216 and (d) N512 Coupling strength ($r_{a,b}\sigma_b$)
843 between daily precipitation and soil moisture (in the top 0.1m of soil) during the southern summer
844 wet season (DJF), over the period 1979-2014. 2-day time lag (i.e. the soil situation 2 days after
845 precipitation) for (e) ERA-Interim, (f) N96, (g) N216 and (h) N512. (i) N216-N96, (j) N512-N216
846 and (k) N512-N96 coupling strength. (l), (m), (n), as for (i), (j) and (k) but with a 2-day time lag
847 between precipitation and soil moisture.

848

849

850

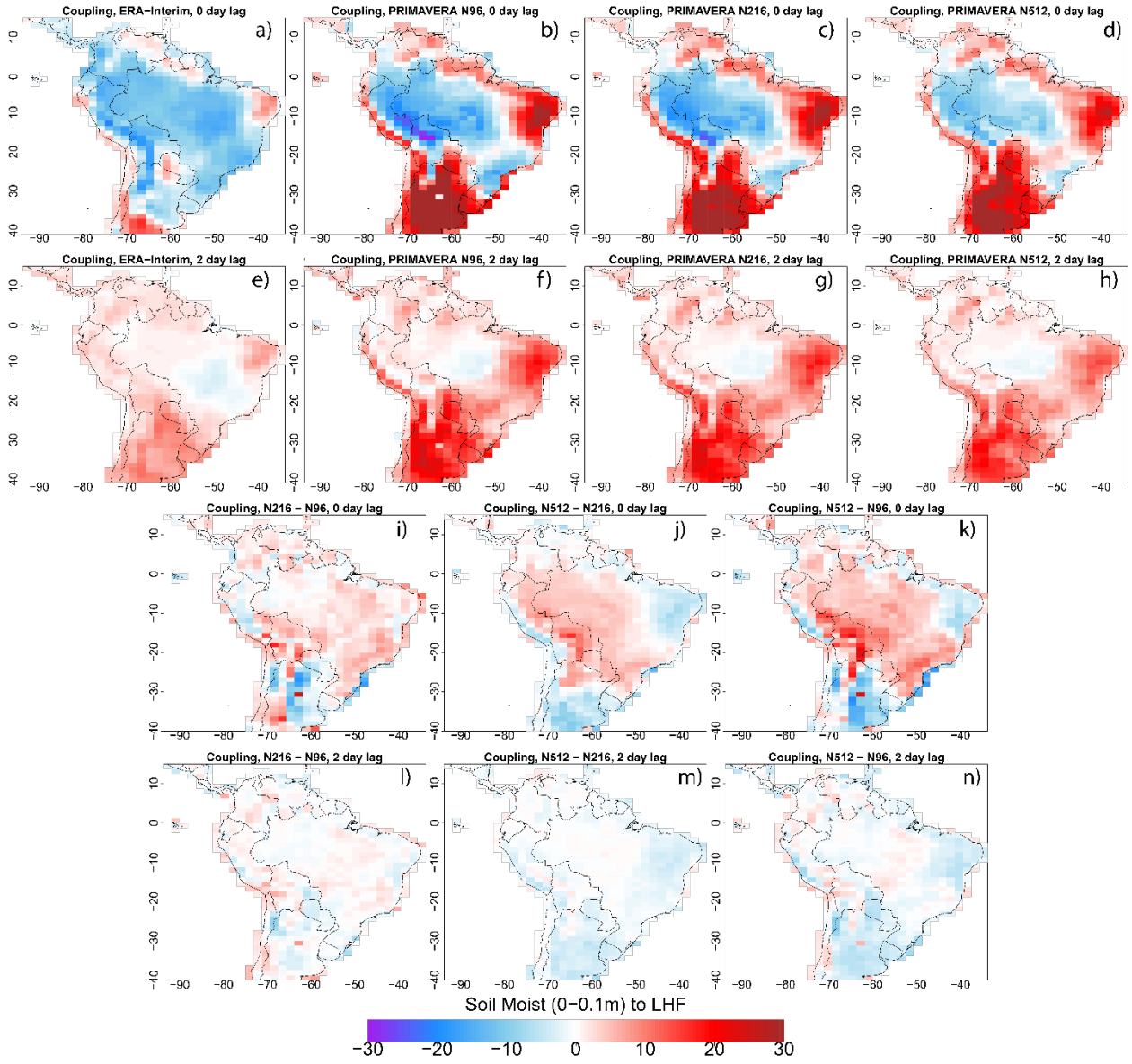

Figure 8: As in Figure 7 but for the coupling strength between daily soil moisture (in the top 0.1m of soil) and latent heat flux (LHF).

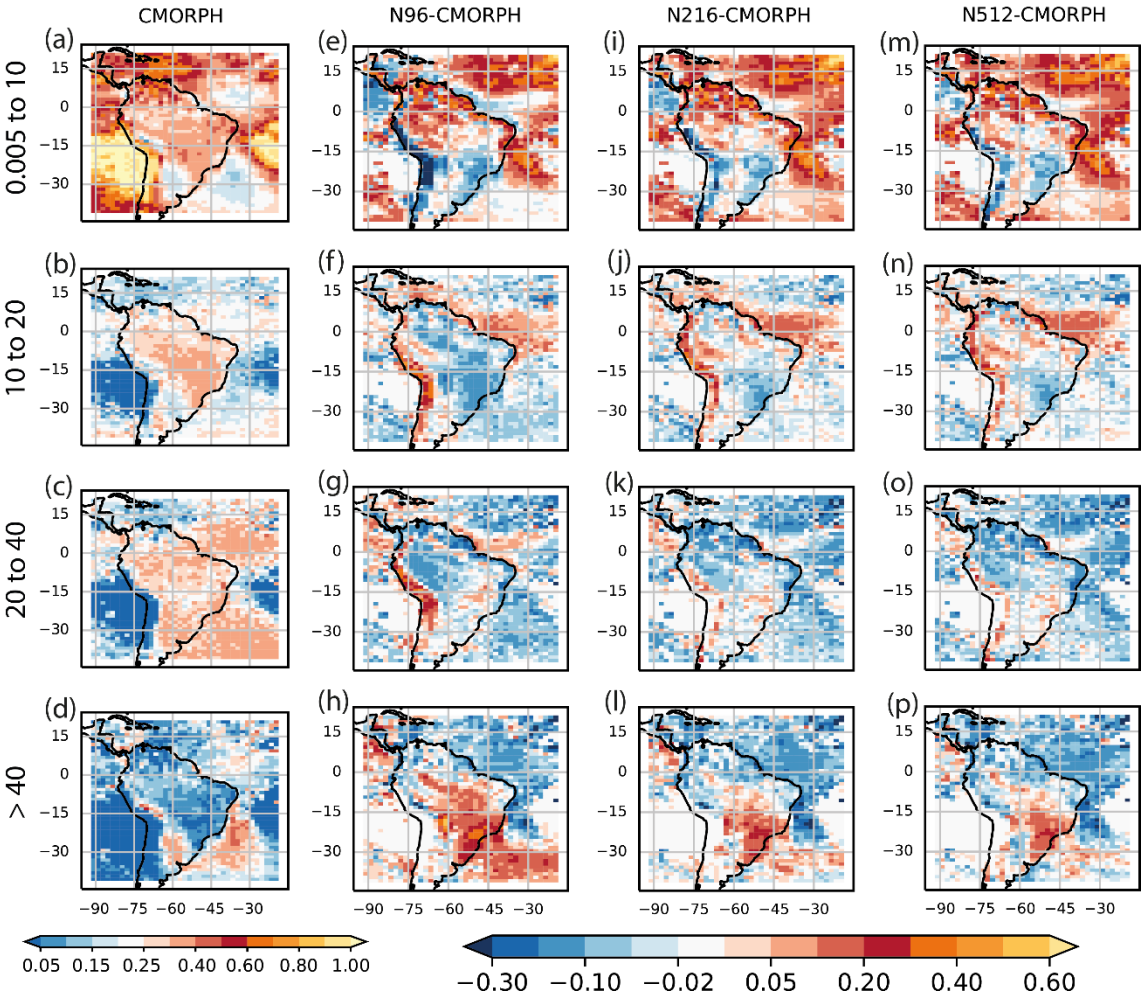

Figure 9: Fractional contribution to the total precipitation from ranges of intensity bins shown in the labels above each panel for CMORPH (a-d) (the sum of each column is unity). Differences in the fractional contributions compared against CMORPH for N96 (e-f), N216 (i-l) and N512 (m-p) all on the N96 common grid. The four ranges of intensity bins are (first row) 0.005 to 10 mm/day, (second row) 10 to 20 mm/day, (third row) 20 to 40 mm/day and (last row) >40 mm.day^{-1}.

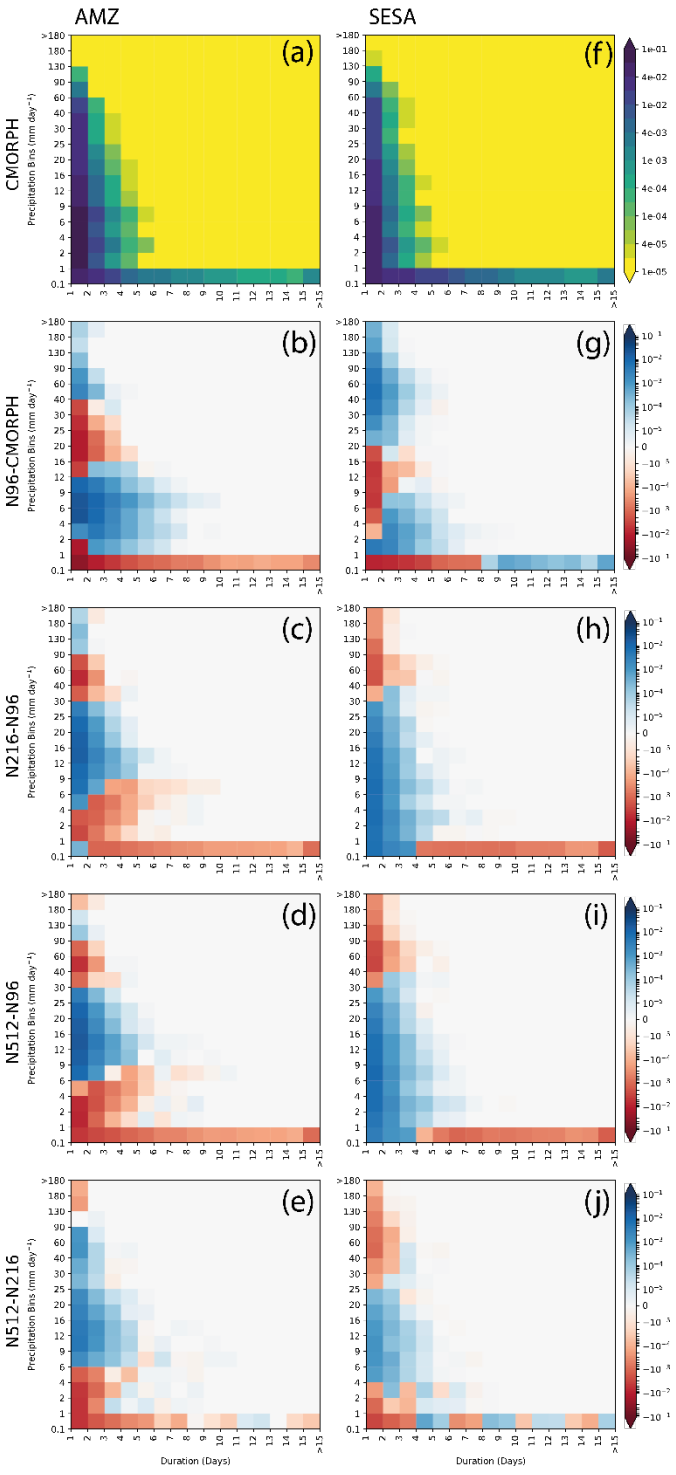

Figure 10: Two-dimensional histograms of binned precipitation lasting for each duration bin, aggregated over all grid points and normalized by the number of spatial and temporal points in each dataset for (a) CMORPH for the AMZ region at N96 grid. Differences between the two-dimensional histograms for (b) N96 minus CMORPH; (c) N216 minus N96; (d) N512 minus N96 and (e) N512 minus N216 computed on the common N96 grid. (f-j) is same as (a-e) but for the SESA region.

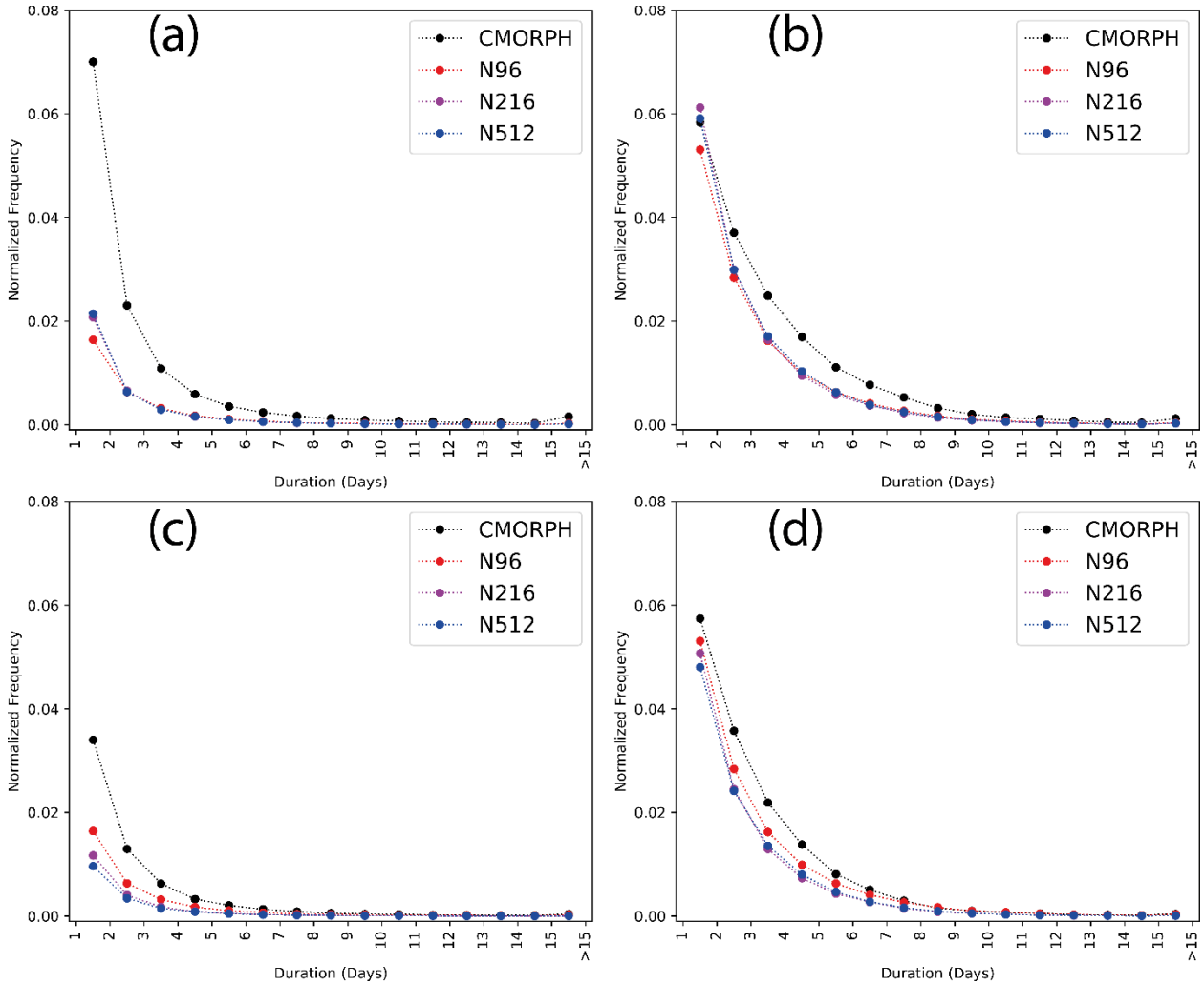

Figure 11: Histograms of dry days (with precipitation less than 0.1 mm day^{-1}) lasting for each duration bin, aggregated over all grid points and normalized by the number of spatial and temporal points in each dataset (a) Amazon and (b) SESA at native resolution for all datasets. (c-d) is same as (a-b) but for datasets on the common N96 grid.

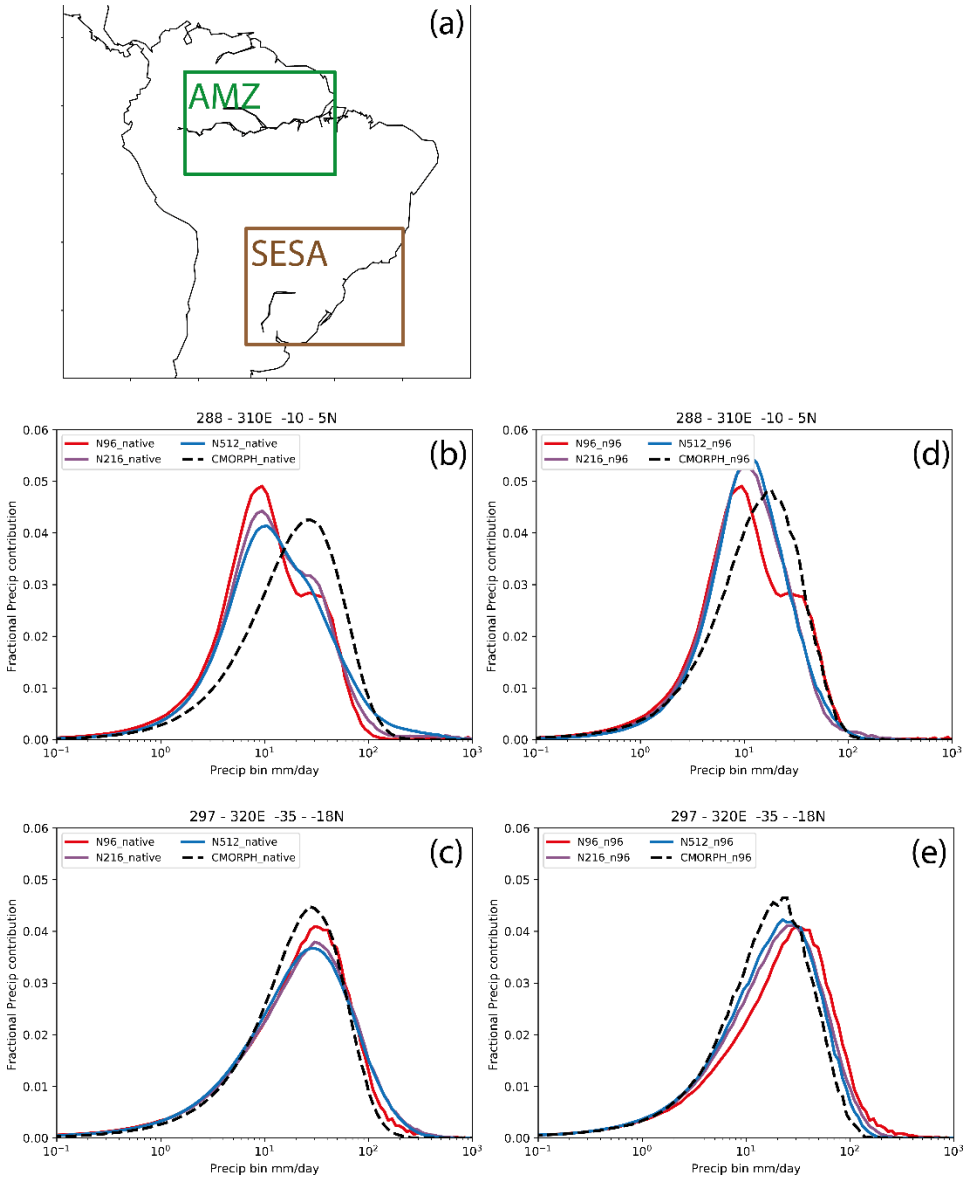

Figure 12: (a) Subregions used in our study (i) the Amazon region (AMZ; green box; 10°S – 5°N; 72°W – 50°W) and (ii) the southeast South America region (SESA; brown box; 35°S – 18°S; 63°W – 40°W). Histograms of the average precipitation contributions to the total precipitation from each precipitation bin for CMORPH and all simulations on their native grids (b) AMZ and (c) SESA. (d-e) is same as (b-c) but at 96 grid.

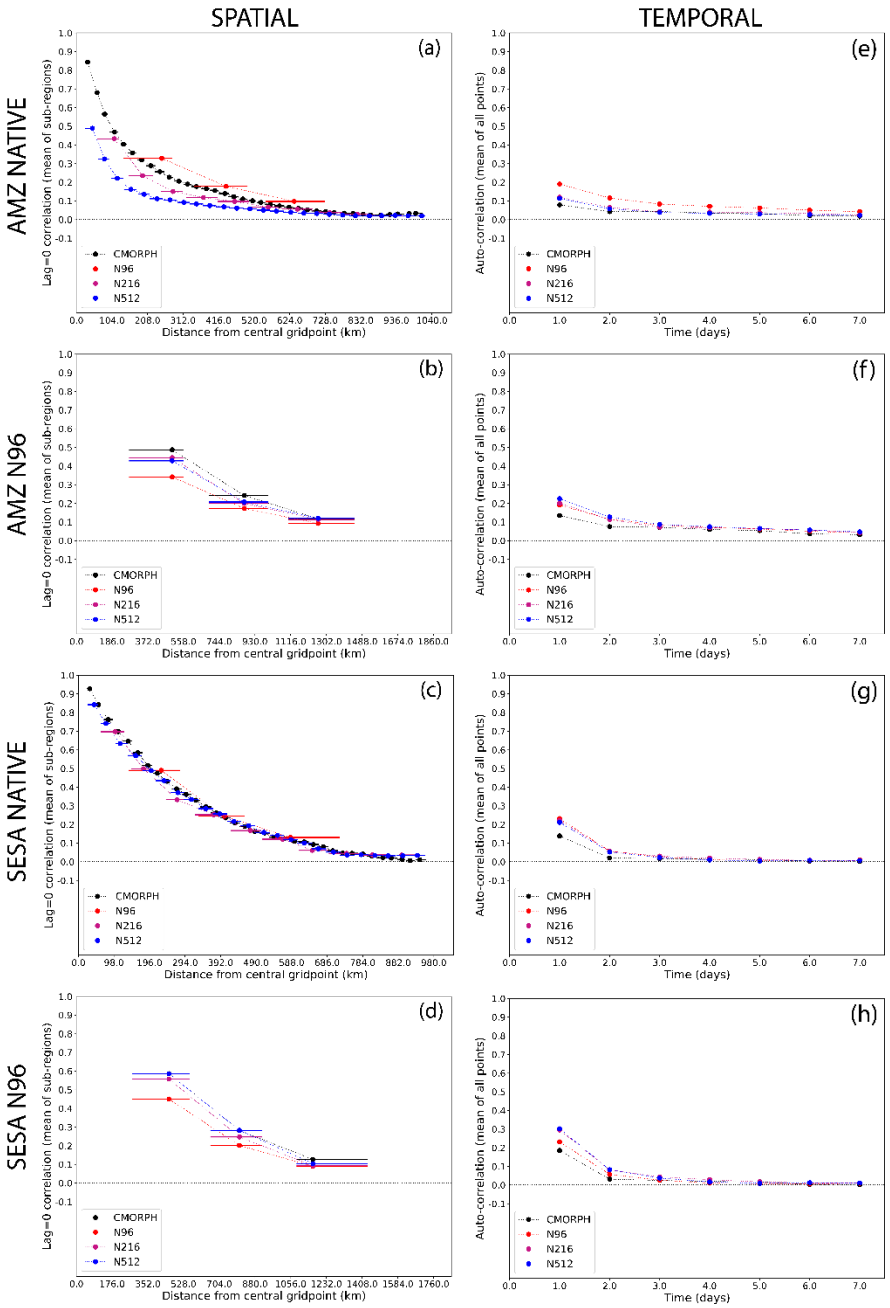

884

885 Figure 13: (a) metric of the spatial scale of daily precipitation (at native resolution), computed by dividing
886 the analysis domain into 1500 km x 1500 km sub-regions and calculating the mean lag-0 correlation
887 between the central grid point and all grid points within each distance bin (which are 1 delta x wide, starting
888 from 0.51x) away from the central grid point, then averaging the correlations over all sub-regions in AMZ;
889 (e) metric of the temporal scale of daily precipitation, computed as the autocorrelation at each point,
890 averaged over all points AMZ. The horizontal lines in (a-d) show the range of distances spanned by each
891 distance bin; the filled circle is placed at the median distance. For clarity, we omit the correlations for zero
892 distance and zero lag, which are 1.0 by definition. (b and f) same as (a and c) respectively for all datasets
893 on the N96 grid; (c-d and g-h) same as (a-b and e-f) respectively but for SESA.